Modeling and Comparative Analysis of CO_2 Absorption Columns in Electrochemical and Thermochemical Carbon Capture Systems

Katelyn Ripley and Fikile Brushett*

Department of Chemical Engineering, Massachusetts Institute of Technology, Cambridge, MA 02139

** Corresponding author email address: brushett@mit.edu*

Abstract

Deployment of post-combustion carbon dioxide (CO_2) capture technologies is needed to reduce emissions from power and industrial sources. Comparisons between existing thermochemical CO_2 capture methods and emerging electrochemical concepts can help contextualize the promise of these new approaches. Here, we investigate the required absorber sizes for three capture systems: amine scrubbing using monoethanolamine (MEA), direct electrochemical (redox-active sorbent), and indirect electrochemical (pH-swing). For the electrochemical systems, we study how column size varies as a function of molecular properties and operating conditions, finding that parameters most closely related to CO_2 uptake rates (i.e., rate constants and pKa) have the greatest impact. Through a Monte Carlo analysis, we find that the direct process can be designed to have column sizes similar to the thermochemical process, however, the CO_2 uptake rate in the indirect process is too slow to enable smaller columns. Broadly, this work connects system input parameters to absorber performance for electrochemical CO_2 capture and provides a foundation for technoeconomic and engineering analyses.

Keywords: post-combustion carbon capture, electrochemical separation, absorption column, redox carrier, pH-swing

1. Introduction

Increasing global energy demand coupled with a reliance on carbon-intensive fossil fuel sources continues to contribute to rising anthropogenic greenhouse gas emissions. While energy use and associated emissions are widely distributed, the global power generation sector alone was responsible for nearly 42% of all carbon dioxide (CO_2) emissions in 2022, resulting in a total of 14.65 Gt of CO_2 released.[1] Renewable energy can help alleviate some of these emissions and is predicted to rise from 29.5% of all global electricity generation sources in 2022 to 41.6% by 2028;[2] however, it is also predicted that coal and natural gas plants will need to continue operating in the short run to meet growing energy needs.[3,4] Thus, these fossil fuels will continue to release CO_2, requiring alternative solutions to limit global warming to 1.5 °C above pre-industrial levels and avert the associated climate consequences.[5] In addition to the power sector, several major industrial processes (i.e., steel, iron, cement, and chemicals manufacturing) are classified as "hard-to-decarbonize," meaning their emissions cannot be easily avoided in the near future, necessitating carbon capture technologies to offset these emissions.[1,6] To incentivize the implementation of carbon capture, utilization, and storage (CCUS) for abating direct emissions from power and industrial facilities, the 2022 Inflation Reduction Act (IRA) increased available tax credits to such facilities performing large-scale CO_2 capture in order to offset the high costs.[7] Such trends in energy demand and government policy encourage the development of a suite of CCUS technologies capable of supporting efforts to meet emission reduction targets.

A range of capture technologies based on chemical absorption,[8] temperature and pressure swing absorption,[9,10] membrane-based separation,[11] and cryogenics[12] have been evaluated for post-combustion capture (PCC) applications where CO_2 is removed and concentrated from flue gas streams (~3-30% CO_2).[13] However, current state-of-the-art, commercialized platforms for large-scale CO_2 capture are typically based on thermochemical absorption and exploit the natural affinity of alkanolamines towards CO_2 at ambient conditions.[14–17] Specifically, when a CO_2-lean amine solution passes through an absorption column, gaseous

CO_2 binds to the amine producing a CO_2-rich solution. This is then pumped to a stripping column where the addition of heat increases the solution temperature and shifts the chemical equilibrium between the solubilized CO_2 and amine molecules to facilitate the release of gaseous CO_2 and the regeneration of the solvent.[18] This process is outlined in **Figure 1a** as four steps: CO_2 capture, sorbent deactivation at elevated temperatures, CO_2 release, and sorbent regeneration by returning to mild temperatures. For amine-based systems, target capture efficiencies are often ~90%,[19,20] however, this is somewhat arbitrarily selected, as cost optimization is required to inform the desired level of capture on a case-by-case basis.[20] Possible amines for use in this process include monoethanolamine (MEA),[21–25] diethanolamine (DEA),[26–29] N-methyldiethanolamine (MDEA),[27–30] diisopropanolamine (DIPA),[26–28,31] piperazine (PZ),[28,30,32–34] and others. MEA, DEA, and DIPA bind up to half a mole of CO_2 per mole of amine, whereas MDEA and PZ can uptake 1 mole of CO_2 per mole.[28,30,32] MEA is the most commonly studied and commercialized alkanolamine due to its low sorbent cost,[35] high rate of reaction with CO_2,[36] and high operating concentrations (i.e., 30–40 wt. % MEA, or 5.1–6.8 M).[8,37–39] Recent studies have investigated the more nascent PZ, as it can absorb CO_2 at a rate 1.5× to 3× faster than MEA and may enable lower regeneration energies.[32] A drawback of using this amine is that it can only achieve solubilities of up to 14 wt. % PZ (~1.6 M), limiting its total CO_2 capacity.[32]

While amine-based absorption processes have the highest technology readiness level (TRL = 9) of all possible capture platforms,[40] the wide temperature swings required for operation (ranging from ~30–40 °C during absorption to ~120 °C during desorption in MEA systems)[38] can lead to amine degradation and limited efficiency.[41] To the latter point, the energetic efficiencies of temperature swing processes are governed by the second law of thermodynamics, in a similar manner to Carnot efficiencies associated with heat engines.[42] Based on a temperature swing between 40 °C to 120 °C, the maximum thermal efficiency achievable (i.e., the Carnot efficiency) is 66.7%, while typically CO_2 capture from flue gas achieves efficiencies in the range of ~19–25%, evincing significant additional energetic losses.[42–45] These low efficiencies cause steam costs to dominate the operating costs for thermochemical CO_2 capture processes

at all flow rates and capture rates.[46,47] In addition to high operating costs, capital costs can be prohibitive, making up anywhere from 5 to 40% of the total costs for industrial-scale capture processes, with as much as 66% of the total capital costs attributed to the absorption column at low CO_2 inlet concentrations.[46] The high column investment costs primarily stem from the large diameters and heights required to process large volumes of flue gas and achieve high (>90%) CO_2 removal.[47] Thus, the combination of high operating costs, high capital costs, and low efficiencies, coupled with the use of fossil fuel derived steam, motivates the investigation of different CO_2 capture technologies.

Recently, electrochemical carbon capture and concentration (eCCC) has been identified as an alternative to the traditional temperature-swing processes. Rather than applying heat to regenerate the solvent, the use of faradaic reactions to selectively reduce or oxidize a redox-active species enables the uptake and release of CO_2 at ambient conditions.[48] Unlike amine-based capture platforms, these technologies have the potential to operate closer to the thermodynamic minimum energy requirement due to the modulation of binding affinities via electrochemical reactions, thereby avoiding the Carnot-like limitations and improving system energy efficiencies.[49,50] Additionally, these processes are modular and are anticipated to scale more easily to meet the demands of a variety of point-source capture sites.[51] Redox-active molecules used in eCCC can either directly bind with CO_2 (i.e., redox-active capture molecules) or indirectly influence the uptake of CO_2 by altering the solution environment (i.e., pH-mediated systems[52–54] or electrochemically-mediated amine regeneration[55–57]). In general, redox-active capture molecules used in "direct" eCCC pathways (**Figure 1b**) exhibit high affinities for CO_2 in the reduced form and low affinities for CO_2 in the oxidized form, facilitating capture and release processes in those respective oxidation states. Research over the past few decades has led to the identification of quinones,[58–62] thiols,[63,64] pyridines and bipyridines,[65,66] transition metal complexes,[58] and other redox-active organic materials[67–70] as possible sorbent species. Molecules for use in direct eCCC are designed for high binding affinity towards CO_2, high CO_2 capacity (i.e., high solubility and a large number of CO_2 molecules bound per molecule of redox species), electrochemical and chemical stability, and resilience in the presence of oxygen (O_2).[71] In the

second type of eCCC process, the "indirect" pathway (**Figure 1c**), a redox-active molecule undergoes an electrochemical reaction but does not directly react with CO_2. Instead, the electrochemically generated molecule can favorably bind with other species in solution (i.e., protons), changing the reaction environment and enabling the capture/release of CO_2. A commonly studied indirect capture process uses a "pH-swing" mechanism, where proton coupled electron transfers (PCETs) can increase and decrease the pH when the redox-active molecule is reduced and oxidized, respectively. At high pH, hydroxides in solution react with CO_2 to form bicarbonate/carbonate solutions, while at low pH, the CO_2 equilibrium favors the gaseous phase and thus trigger the release of CO_2. Molecules studied for use in this process include quinones,[52,72] phenazines,[73,74], redox-active amines,[75] and inorganic compounds.[67,76,77] As with the direct capture molecules, the indirect capture species must exhibit electrochemical and chemical stability in the presence of all flue gas components (i.e., O_2), but they are also designed to have high pKa values and high solubility at all pH conditions.[67] For both processes, molecules can be dissolved in an electrolyte or immobilized on an electrode surface, however, for the purposes of this work, we solely consider solubilized species. A key difference between these electrochemical approaches is that typical direct capture processes leverage nonaqueous solvents to avoid the possibility for protons in solution to compete with CO_2 uptake (*vide infra*),[78] while indirect pH-swing processes occur in aqueous environments. Here, we limit our discussion to these canonical solvent conditions; however, they are not necessarily a requirement of either system. In the future, altering such conditions may prove to be a viable option for process innovation.[79]

The feasibility of both direct and indirect eCCC processes has been demonstrated at the laboratory scale through successful molecular discovery and proof-of-concept campaigns.[54,61,72,73,80–82] These efforts must be complemented and contextualized by additional engineering analyses to investigate how these new approaches can best be leveraged to operate efficiently across various scales. Specifically, studies informing the required molecular properties and operating conditions necessary for technical and economic viability at practical scales can be used to identify knowledge gaps, navigate the complex design space, and effectively allocate resources. The cost and energy benchmarks set by commercialized thermochemical

capture systems provide targets upon which the performance of these electrochemical systems can be compared, thus offering an initial measure of potential competitiveness. To this end, thermodynamic studies have shown that the electrochemical system level energy requirements are comparable to, if not better than, those reported for state-of-the-art absorption-based PCC.[49,50,54,56] Typical thermochemical system regeneration energies fall within 106 – 220 kJ mol^{-1} while electrochemical systems have been reported to range from 33.2 – 90 kJ mol^{-1}.[76,83–86] In addition, these reports have identified several possible system architectures consisting of 2–, 3–, and 4–stage configurations.[49,50] In the "4–stage" configuration, regardless of the capture mechanism used, the redox-active molecules are first activated in an electrochemical cell via an electroreduction reaction and the solution is pumped to the absorption column where CO_2 uptake occurs. The CO_2-bound redox-active molecule then flows to the anode where an electrooxidation reaction shifts the equilibrium towards gaseous CO_2. Finally, the solution passes on to a desorption unit (i.e., a flash tank) for CO_2 release in a concentrated stream and the cycle is repeated. In addition to the 4–stage configuration, designs that eliminate the absorber (thus enabling cathodic absorption), flash tank (thus enabling anodic desorption), or both have been proposed as 3– or 2–stage configurations.[49,50] In order to establish engineering frameworks upon which we can directly compare thermochemical systems to their emerging electrochemical counterparts, we elect to focus on the 4–stage configuration because of its direct correlation to the 4 stages in the amine-scrubbing process (**Figure 1a**).

Despite the overlap in required unit operations between thermochemical and electrochemical capture platforms, to our knowledge, detailed comparisons in the design of such units have not been extensively studied. Specifically, it is presently unclear if the large absorption columns associated with thermochemical PCC will also apply to 4–stage eCCC. If the required absorption column for capturing CO_2 from a flue gas stream using an electrochemical system is smaller than that for its thermochemical counterpart, the resulting capital cost reduction may further incentivize eCCC development. Alternatively, if the sizes are comparable, there may be options for eventual brownfield installations of the eCCC systems (i.e., using decommissioned absorption columns or retrofitting existing infrastructure with new and improved capture technologies),

thus avoiding new capital investments. Further, establishing connections between material properties, operating conditions, and absorption column size for eCCC systems may offer design guidance to chemical scientists. While traditional amine-based capture processes have been extensively studied and their full system performance (i.e., integration of the absorption columns, stripping columns, and heat exchangers) optimized to the point that amine concentration, CO_2 loading into the absorption column, and flow rates have all been set to minimize total costs, 4–stage electrochemical systems have not yet matured. To inform column design in such eCCC systems, it is necessary to develop an understanding of the 4–stage process and derive material balances associated with the entire electrochemical system to determine required system flow rates and species concentrations entering and leaving the column.

Here, we develop a comprehensive absorption column model that calculates the tower size required to capture and release a desired amount of CO_2 in both eCCC and thermochemical systems. Due to the relative nascency of electrochemical capture platforms, we construct this generalized absorption column model in MATLAB to enable flexibility in the chosen redox-active species and associated electrolyte. We subsequently use the model to investigate how changes in molecular properties such as CO_2 absorption kinetics, capture species solubilities, and equilibrium relationships as well as select system operating conditions can impact the absorption column size. We then perform a Monte Carlo sensitivity analysis on the direct and indirect eCCC input parameters to assess the likelihood that the eCCC absorption column packing volumes can be less than or equal to those of thermochemical capture columns required to capture the same amount of CO_2 from the same flue gas streams. From these results, we identify desirable molecular properties for future electrolyte engineering efforts and discuss the possibility of downsizing or retrofitting state-of-the-art thermochemical platforms. While not the focus of this work, the model developed here sets the groundwork for future system level analyses (i.e., cost comparisons) that will integrate the absorption column performance with that of the electrochemical cell / stack and the desorption units.

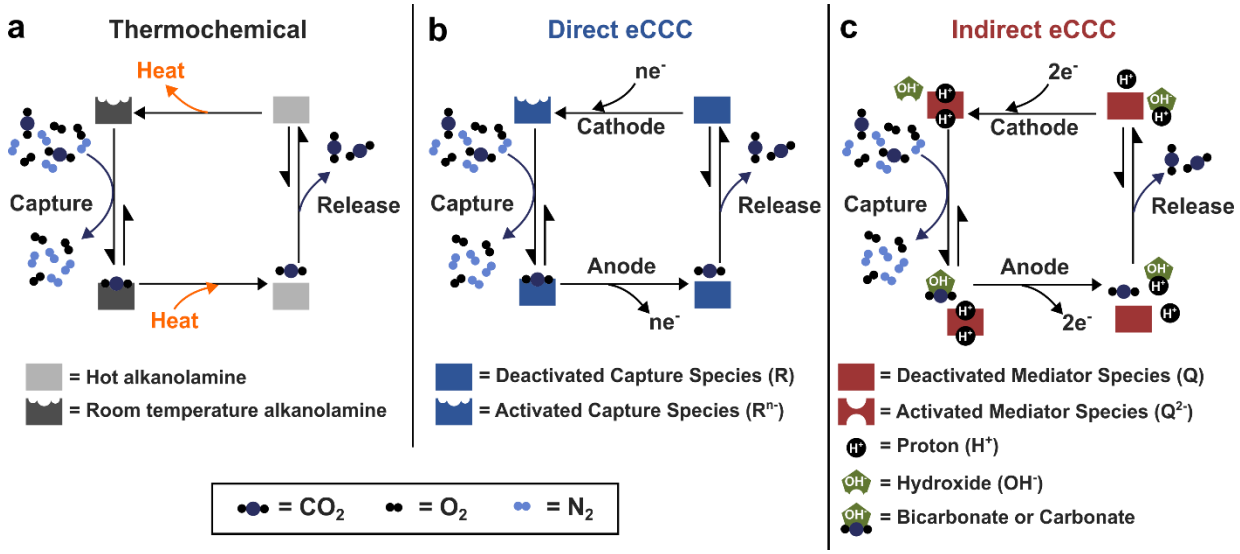

Figure 1. Process descriptions of (a) alkanolamine-based thermochemical capture, (b) direct eCCC, and (c) indirect eCCC processes. The indirect eCCC process shown here represents a pH-swing process.

2. Process Description

2.1. Overall Process Description

For both eCCC processes, the 4–stage system configuration consists of an electrochemical reactor, an absorption column, and a desorption unit such as a flash tank (**Figure 2a**). A CO_2-rich effluent stream exiting a power plant or industrial facility (i.e., cement or steel process) first enters the bottom of the absorption tower (Stream 1) where the gaseous CO_2 is absorbed by a solubilized sorbent species. This gas effluent stream is well defined due to knowledge of the process emissions that stem from point source facilities. After CO_2 is removed, the CO_2-lean gas stream (Stream 3) exits from the top of the column. The CO_2-rich liquid stream passes through the electrochemical reactor where the sorbent/solution affinity towards CO_2 is diminished via an electro-oxidation reaction, enabling the release of a pure CO_2 stream from the flash tank unit (Stream 5) for storage or utilization. The liquid solution is then passed through the cathode of the electrochemical cell for sorbent regeneration via an electro-reduction reaction to repeat the cycle.

To compare the size of eCCC absorption columns with those used in previously investigated thermochemical processes, we design a system capable of separating the same amount of CO_2 (i.e., achieving the same capture fraction, α) as a representative thermochemical system. For these processes, α is calculated according to **Eq. 1**, where $\bar{V}_m$ (mol h^{-1}) is the total molar flow rate of the vapor stream, m, and y_{m,CO_2} (–) is the mole fraction of CO_2 in vapor stream, m.

$$\alpha = \frac{\text{CO}_2 \text{ removed from the flue gas}}{\text{Total CO}_2 \text{ entering the column}} = \frac{\bar{V}_5 y_{5,CO_2}}{\bar{V}_1 y_{1,CO_2}} = 1 - \frac{\bar{V}_3 y_{3,CO_2}}{\bar{V}_1 y_{1,CO_2}} \quad (1)$$

From the known inlet flue gas properties (y_{1,CO_2} and $\bar{V}_1$), the overall material balances across the gas streams (i.e., Streams 1, 3, and 5 as indicated by the light blue dashed box in **Figure 2a**), and α can all be used to define the remaining unknown gas stream variables ($\bar{V}_3$, $\bar{V}_5$, and y_{3,CO_2}). The full gas-phase material balances are outlined in **Section S.1** of the **Supporting Information (SI)**. To determine the absorption

column size required to achieve α, we must use this information and other operating conditions to also predict the flow rates and species concentrations in the liquid streams. While we are most interested in the material balances around the absorption unit (green dashed box in **Figure 2a**), material balances about all process units must be evaluated for both the direct and indirect capture process to ensure that the conditions and molecular parameters provided can achieve the desired capture fraction.

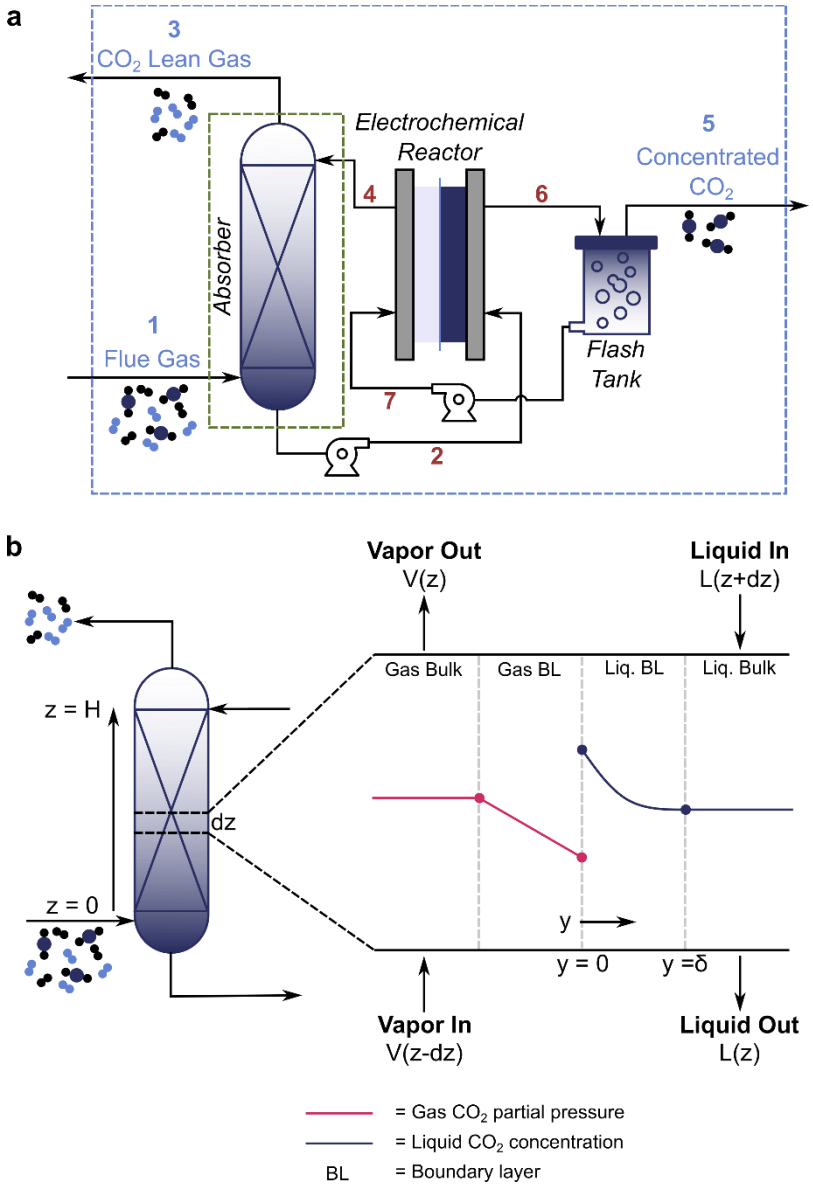

Figure 2. (a) Schematic of a 4–stage electrochemical CO_2 capture process. The blue dashed box represents the material balance on the gas streams and the green dashed box represents the material balance on all streams entering and leaving the absorption column. (b) Detailed view of the schematic used to model

concentration profiles along the length of the absorption column and of the two-film region that is required to model the mass transport between the gas and liquid phases within the column.

2.2. Direct Capture Process: Overview and Material Balances

The absorption mechanism in direct eCCC processes typically follows the subsequent set of reactions (**Eq. 2 – Eq. 5**) to bind and release CO_2.

$$\mathrm{R} + ne^- \rightarrow \mathrm{R}^{n-} \tag{2}$$

$$\mathrm{R}^{n-} + q\mathrm{CO_2} \xleftrightarrow{K_{1,direct}} \mathrm{R(CO_2)}_q^{n-} \tag{3}$$

$$\mathrm{R(CO_2)}_q^{n-} \rightarrow \mathrm{R(CO_2)}_q + ne^- \tag{4}$$

$$\mathrm{R(CO_2)}_q \xleftrightarrow{1/K_{2,direct}} \mathrm{R} + q\mathrm{CO_2} \tag{5}$$

Where R represents a generic capture species in the direct capture process, n is the number of electrons transferred per mole of R reduced or oxidized, q is the number of moles of CO_2 taken up per mole of capture species, $K_{1,direct}$ (–) is the binding affinity of the capture species towards CO_2 in the reduced/activated state $\left(K_{1,direct} = \frac{[\mathrm{R(CO_2)}_q^{n-}][C_0]}{[\mathrm{R}^{n-}][\mathrm{CO_2}]^q}\right)$, and $K_{2,direct}$ (–) is the binding affinity of the capture species towards CO_2 in the oxidized/deactivated state $\left(K_{2,direct} = \frac{[\mathrm{R(CO_2)}_q][C_0]}{[\mathrm{R}][\mathrm{CO_2}]^q}\right)$. For direct eCCC processes, $K_{1,direct} \gg K_{2,direct}$ to facilitate capture and release at different oxidation states, but the exact values of these binding constants vary across sorbents and electrolytes. In the equilibrium expressions, $[C_0]$ is the standard concentration (1 M).

As mentioned earlier, in some cases the nucleophilic capture molecules may have pKa values greater than that of water, leading to protonation in place of CO_2 uptake under aqueous conditions. For example, according to Simpson and Durand, the rate of protonation of the anthraquinone dianion is twice that of the rate of CO_2 uptake.[62] For such molecules, this necessitates that the capture species is dissolved in organic, aprotic solvents such as dimethylformamide (DMF), dimethyl sulfoxide (DMSO), propylene carbonate

(PC), or acetonitrile (ACN) to maximize capture species utilization.[87] To enable rapid ion mobility for electroanalytical studies, many experiments have been performed in DMF or ACN;[80,88,89] however use of these solvents at scale may be challenging due to their toxicity and volatility, respectively. As such, in this work, we explore the utilization of PC as the solvent.

Many direct capture molecules can undergo 2-electron transfers ($n = 2$); however, the value of q varies between 1 or 2 depending on the binding strength of the radical anion ($R^{\bullet -}$) towards CO_2.[68] Consequently, the mechanism by which these capture molecules bind with CO_2 can follow an ECEC/ECE[62,69,89,90] or EEC[91–93] mechanism, where "E" represents electrochemical reactions and "C" represents any chemical reactions with CO_2. As values for the dianion binding affinity towards CO_2 ($K_{1,direct}$) are widely available across literature, we assume an EEC mechanism in this work. This also allows us to estimate an upper bound of column sizing given the lower CO_2 capacity of the sorbent species.

Despite the CO_2 uptake reaction in the absorption column being of a similar form to that observed in amine-based thermochemical capture processes ($A + CO_2 \overset{k_1}{\rightarrow} B$), extensive kinetic studies investigating the CO_2 uptake (or homogeneous reaction) rates have yet to be performed across all relevant eCCC sorbent molecules. The few studies that have been conducted suggest a second-order rate constant, $k_{1,f,direct}$ (M^{-1} s^{-1}), which varies across two orders of magnitude (ca. 6-661 M^{-1} s^{-1}) depending on the sorbent species, solvents, and supporting salts.[62,82,90] This range of rate constants is significantly lower than the reported rate constants between MEA and CO_2 ($k_{1,f,MEA} \approx 5868$ M^{-1} s^{-1} at room temperature).[94–96] However, these studies focused on strong nucleophiles (i.e., benzoquinone, anthraquinone, naphthoquinone, phenanthrenequinone, etc.) with $q = 2$ and the reported rate constants were measured only after reduction to the semiquinone (i.e., for the first CO_2 uptake reaction).[62,82,90] We hypothesize that if the rate constants associated with the uptake of CO_2 after full reduction to R^{n-} were measured, they would be larger due to the increased nucleophilicity of the sorbent species.[82] Accordingly, we assume that, for EEC mechanisms, the rate constants listed above serve as a lower bound. This assumption may be revisited once additional experimental studies are

performed to measure the rate of reaction between CO_2 and the dianion for molecules exhibiting EEC mechanisms. Further, if the rates of reaction between CO_2 and the capture molecule impact process viability, molecular design campaigns can be pursued to engineer species with faster uptake rates. In this work, we focus on addressing the impacts of these uncertain rate constants on the direct eCCC absorption column size.

Given these model conditions and the anticipated importance of reaction rate on the column size, we develop a set of governing equations for the entire capture process (i.e., absorption column, electrochemical reactor, and flash tank) to ensure the requirements of the electrochemical cell are met while simultaneously achieving the desired capture fraction. Across all unit operations, the total concentration of capture species, $[R_{tot}]$ (mol L^{-1}) must remain constant and thus we define this as the sum of R in all process-relevant states (**Eq. 6**).

$$[R_{tot}] = [R^{n-}] + [R] + \left[R(CO_2)_q^{n-}\right] + \left[R(CO_2)_q\right] \quad (6)$$

As with other electrochemical systems (e.g., batteries) and prior eCCC literature,[49,50] we define the state-of-charge of the direct capture process, $x_{a,direct}$ (–), as the fraction of capture species in its activated (a) state (**Eq. 7**).

$$x_{a,direct} = \frac{[R^{n-}]+[R(CO_2)_q^{n-}]}{[R_{tot}]} \quad (7)$$

With each single pass of the electrolyte through the electrochemical cell (or stack), it is possible to control this state-of-charge through the passage of current. Given that the electrochemical cell is not the focus of this discussion, we opt to symmetrically adjust the state-of-charge around 0.5, setting the upper and lower bounds on the state-of-charge as $x_{a,direct}$=0.5 $\pm \frac{\Delta x_a}{2}$.[50] While the state-of-charge remains constant within the absorption column where no electrochemical reactions occur, it will increase and decrease across the cathode and the anode, respectively, to enable the capture and release of CO_2 in the absorption column and flash tank that follow.

Beyond these electrochemical relationships, the flux of CO_2 into and out of the system requires additional carbon balances. The 4–stage system is designed so that CO_2 only enters/leaves the solution in the absorber/flash tank. Consequently, we define a CO_2 balance where the total dissolved inorganic carbon (DIC, mol L^{-1}) is constant across the cathode and anode. The expression for DIC in stream *m* is shown in **Eq. 8**.

$$\mathrm{DIC}_{m,direct} = [\mathrm{CO_2}]_m + q\left[\mathrm{R(CO_2)_q^{n-}}\right]_m + q\left[\mathrm{R(CO_2)_q}\right]_m \quad (8)$$

For the DIC across the anode and the cathode to be constant (i.e., DIC_7=DIC_4 and DIC_2=DIC_6), the liquid phase volumetric flow rate must be constant across all process units. This is only true if the solution is dilute in the absorbate, CO_2. The maximum CO_2 concentration in a PC-based solution is limited to ~0.103 mol L^{-1} bar^{-1} at room temperature,[97] thus, assuming only PC and CO_2 in solution, its liquid-phase mole fraction will not exceed 0.007 (the presence of a supporting salt may further lower this value). This low concentration validates that we can assume constant liquid flow rate without loss of generality.

To achieve the preset capture efficiency and encapsulate the uncertainty in CO_2 uptake rates, we cannot assume both chemical (i.e., $K_{1,direct}$ and $K_{2,direct}$) and phase (i.e., Henry's Law) equilibrium along the height of the absorber, as has been done in prior eCCC models.[49,50] Rather, we calculate the total CO_2 exchanged between phases through a rate-based absorption column model reliant on changing reaction rates and interfacial fluxes. Given the uncertainty in the reaction rate constants and the impact that both mass transfer and kinetics will have on the column concentration profiles, the liquid stream outlet conditions will likely deviate the most from its equilibrium state. To appropriately size the column to achieve the specified CO_2 uptake and release, we choose to relax one of the equilibrium assumptions at the liquid outlet and apply the material balance in **Eq. 9**, where $\dot{Q}_L$ (m^3 h^{-1}) is the solution volumetric flow rate. A similar balance can be written around the flash tank without the additional gas inlet term; however, for that unit we can assume both chemical and phase equilibrium, as flash tanks are single-equilibrium-stage units.[98]

$$\dot{Q}_L\left(\mathrm{DIC}_{4,direct}\right) + \bar{V}_1 y_{CO_2,1} = \dot{Q}_L\left(\mathrm{DIC}_{2,direct}\right) + \bar{V}_3 y_{CO_2,3} \quad (9)$$

By relaxing either the assumption of chemical equilibrium or phase equilibrium, we generate two extreme estimates of CO_2 concentration at the liquid outlet of the absorption column. Adhering to Henry's law to achieve phase equilibrium establishes an upper bound on CO_2 concentration, while achieving chemical equilibrium sets the lower bound. Consequently, we can selectively choose which constraint is enforced depending on the absorption column conditions. This decision-making process will be further discussed in **Section 4.2** (*vide infra*). The full derivation of relevant material balances for the 4–stage process is available in **Section S.2** of the **SI**.

2.3. Indirect Capture Process: Overview and Material Balances

An alternative eCCC method is via pH-swing mechanisms that exploit the natural equilibrium between CO_2 and aqueous solutions.[48,71] Rather than a redox-active sorbent species, these "indirect capture processes" require a redox-active species to undergo a proton coupled electron transfer (PCET) to enable the removal/release of a proton upon reduction/oxidation, respectively. The mechanism for indirect capture typically follows **Eq. 10 – Eq. 13**, where Q represents a generic redox-active mediator species, $K_{1,indirect}$ (–) is the equilibrium constant between CO_2 and bicarbonate (HCO_3^-), $K_{2,indirect}$ (–) is the equilibrium constant between HCO_3^- and carbonate (CO_3^{2-}), and K_w (~1×10^{-14}, –) is the water dissociation constant into proton (H^+) and hydroxide (OH^-) ions. **Eq. 11a, b** and **Eq. 13a, b** represent the CO_2 uptake and release steps in the process, respectively.

$$\mathrm{Q} + ne^- + n\mathrm{H}^+ \rightarrow \mathrm{QH}_n \quad (10)$$

$$\mathrm{OH}^- + \mathrm{CO}_2 \xleftrightarrow{K_{1,indirect}/K_w} \mathrm{HCO}_3^- \quad (11a)$$

$$\mathrm{HCO}_3^- \xleftrightarrow{K_{2,indirect}} \mathrm{CO}_3^{2-} + \mathrm{H}^+ \quad (11b)$$

$$QH_n \rightarrow Q + nH^+ + ne^- \quad (12)$$

$$CO_3^{2-} + H^+ \overset{1/K_{2,indirect}}{\longleftrightarrow} HCO_3^- \quad (13a)$$

$$HCO_3^- + H^+ \overset{1/K_{1,indirect}}{\longleftrightarrow} CO_2 + H_2O \quad (13b)$$

For many mediator species studied in pH-swing capture process, the number of electrons transferred, n, is typically 2, and thus we will only consider such cases here.[52,53,73,99] The first CO_2 uptake step (**Eq. 11a**) is written with hydroxides as opposed to protons due to 1) the likelihood that the solution pH will be high to accelerate the absorption reactions and 2) the rate-limiting reaction is the conversion of CO_2 and OH^- to HCO_3^-.[100,101] These equilibria and rate constants are well-studied due to their relevance to ocean acidification and CO_2 mineralization.[102]

Because the rate of reaction in the column is limited by the interaction between OH^- and CO_2, the accessible pH after deacidification (reduction) will have a significant effect on the absorber size. Consequently, achieving a high pH is desirable; however, it is unlikely that the mediator species will fully protonate to QH_2, as the degree of protonation relies on the acid dissociation constants ($K_{a,1}$ and $K_{a,2}$, –) of the mediator species. The generalized mechanism above suggests that Q completely reduces and converts to QH_2, however, to generalize the model for a variety of redox species, we assume that the reduced species equilibrate with protons according to the relationships in **Eq. 14** and **Eq. 15**.

$$QH_2 \overset{K_{a,1}}{\longleftrightarrow} QH^- + H^+ \quad (14)$$

$$QH^- \overset{K_{a,2}}{\longleftrightarrow} Q^{2-} + H^+ \quad (15)$$

Reduced mediator species with high pKa values ($pKa = -\log(K_a)$) have an increased affinity for protons in solution, enabling broader pH swings. Generally, if the pH of the solution is greater than the pKa

of a species, proton dissociation will be favored. In addition to the pKa, buffering via the bicarbonate and carbonate species in solution will limit the pH change and must be accounted for in the model.

Given the dependency of CO_2 uptake rate on system pH, we follow a similar framework to that developed in the direct capture process (**Section 2.2**) to appropriately account for CO_2 balances around the absorber. Specifically, we apply identical material balance constraints (i.e., constant DIC in the electrochemical reactor and constant state-of-charge in the absorption column and flash tank). For the indirect capture process, we can define the total mediator species concentration ($[Q_{tot}]$), state-of-charge ($x_{a,indirect}$), and DIC for a single stream, m, as shown in **Eq. 16** – **Eq. 18**.

$$[Q_{tot}] = [Q^{2-}] + [QH^{-}] + [QH_2] + [Q] \tag{16}$$

$$x_{a,indirect} = \frac{[Q^{2-}]+[QH^{-}]+[QH_2]}{[Q_{tot}]} \tag{17}$$

$$DIC_{m,indirect} = [CO_2]_m + [HCO_3^{-}]_m + [CO_3^{2-}]_m \tag{18}$$

As with the direct capture process, prior indirect system material balances have assumed that all streams achieve equilibrium within the absorption column.[54] To relax this assumption and account for the CO_2 uptake rates in the column, we use **Eq. 9** and its equivalent form in the flash tank to appropriately balance the CO_2 entering/ leaving the units as well as choose whether to constrain chemical or phase equilibrium in the stream leaving the column. According to Wallin and Olausson, the uptake of CO_2 into alkaline aqueous solutions at room temperature occurs with a second-order rate constant of 8332 M^{-1} s^{-1} while the rate constant for CO_2 absorption in MEA systems is around 5868 M^{-1} s^{-1}.[94,101] Despite the fact that these are of the same order of magnitude, the CO_2 uptake reactions in basic (pH ~14) solutions occur at lower OH^{-} concentrations (~1 M) than those of MEA systems (typically, ~5 M). Consequently, it is likely that the rates of reaction in the indirect eCCC process (dictated by the multiplicative product of the active species concentrations and the rate constant) will be slower than amine capture systems. While it may be possible

to elevate the hydroxide concentrations by adding base to the solution (and thus allowing for faster rates of reaction), we do not consider this in the present work due to prior observations that excessive base can prevent the release of sufficient CO_2.[103] To account for the anticipated slower uptake kinetics, we chose to constrain the absorber outlet to achieve CO_2 phase equilibrium (i.e., satisfy Henry's law) while relaxing $K_{1,indirect}$. All other equilibria (K_w, $K_{2,indirect}$, $K_{a,1}$, and $K_{a,2}$) apply at all stages in the column. The accuracy of these assumptions will be discussed in **Section 4.3** (*vide infra*).

In addition to the above relationships, the indirect process involves the dynamic exchange of protons between hydroxides, bicarbonates, carbonates, and reduced forms of the mediator species to maintain their equilibria, resulting in the definition of a total alkalinity (TA, mol L^{-1}), shown here for a single stream, *m* (**Eq. 19**).[104]

$$\mathrm{TA}_m = [\mathrm{HCO_3^-}]_m + 2\left[\mathrm{CO_3^{2-}}\right]_m + [\mathrm{OH^-}]_m + 2\left[\mathrm{Q^{2-}}\right]_m + [\mathrm{QH^-}]_m - \left[\mathrm{H^+}\right]_m \quad (19)$$

When current is applied across the electrochemical reactor, the TA will change as electrons are added/removed from the system to enable shifts in the pH. We can use the relationships in **Eq. 20** and **Eq. 21** to capture the change in TA across the cathode and the anode, respectively.

$$\mathrm{TA}_4 - \mathrm{TA}_7 = n\mathrm{Q}_{tot}\Delta x_a \quad (20)$$

$$\mathrm{TA}_2 - \mathrm{TA}_6 = n\mathrm{Q}_{tot}\Delta x_a \quad (21)$$

As no electrons transfer to or from the solution in the absorption column and the flash tank, the TA must be constant in those process units to maintain the charge balance. The full derivation of the material balances used to estimate the outlet concentration from the absorption column can be found in **Section S.3** of the **SI**.

3. Absorption Column Sizing: Model Development

The simultaneous physical absorption of CO_2 coupled with the reactive uptake of CO_2 by dissolved reactants requires a rate-based, reactive absorption model that describes the change in concentrations along

the column length.[98] While Aspen Plus® or other process engineering software packages are well-equipped to incorporate system thermodynamics into reactive absorption column design, the unique application of this column to an electrochemical process requires frameworks not readily available or easily adaptable in such software (i.e., electrochemical unit operations and the flexibility to quickly study a wide variety of sorbent species). Consequently, we use prior reports of absorption column design equations to build an in-house column sizing model for use in both thermochemical and electrochemical systems, which we validated against well-studied systems (i.e., amine-based CO_2 capture processes).

Amine-based capture technologies were first introduced in the 1930s and have become the state-of-the-art approach for PCC.[105,106] Over the past several decades, the growing interest in such platforms to remove CO_2 from point source process emission streams has led to extensive investigation of absorption column design via experimental and modeling efforts. Practitioners have developed libraries of physicochemical properties and reaction rates/mechanisms for a range of alkanolamines to aid in the accurate study and optimization of absorption columns that utilize these chemistries. Specifically, the CO_2 reaction kinetics,[94,95,107] diffusivities,[108] solubility,[8,37,38] viscosity,[109] density,[39,110] and other material properties of the most commonly used amine, MEA, have been well-documented, enabling a detailed understanding of molecular interactions for process modeling and cost studies.[111] MEA-based absorption columns implemented at the bench-, pilot-, and industrial-scale have allowed researchers to investigate absorption column concentration and temperature profiles as well as overall performance.[38,112–115] Additionally, modeling work to assist in designing relevant and optimized columns at various scales has been established and well-validated for MEA systems.[22,38,116] While such modeling approaches differ in complexity, they provide a valuable knowledge base that can be leveraged in the pursuit of new CCUS materials and applications.

Many early absorption column models assume a simple equilibrium-stage model; however, when an absorber is physically operated, the internal theoretical stages do not achieve equilibrium conditions due to

kinetic and mass transfer limitations.[117–119] To address this, rate-based models using film, penetration, or surface renewal theories have been developed to capture both reaction kinetics and interfacial mass transfer dynamics.[120,121] Prior models developed for MEA-based CO_2 absorbers consistently exploit such rate-based dynamics; however, because the reaction between MEA and CO_2 is assumed to be an irreversible, pseudo-first order reaction, analytical solutions can be obtained via the definition of enhancement factors (ratio of mass transfer coefficients with and without reaction) and Hatta numbers (ratio between diffusion and reaction time).[121,122] While this simplifies many MEA-based reactive absorption models, it is uncertain if emerging eCCC processes will follow the same irreversible, pseudo-first order kinetics. Thus, we elect to focus on numerical solutions to the rate-based absorber model to enable functionality for reactions that could be reversible and second-order. The adapted model can predict the diameter and height of both thermochemical and eCCC process columns by adopting a combined plug-flow reactor model with a two-film reaction-diffusion framework (**Figure 2b**). To ensure flexibility, the model is generalized to match the uncertainty surrounding both direct and indirect eCCC capture methods. We also incorporate separate sets of expressions and correlations for random and structured packing materials to enable future investigations into the effects of packing material properties and costs.

3.1. Absorption Column Sizing Model: Diameter

To size the absorber accurately, we must first calculate the column diameter, as the column height depends on the cross-sectional area. This diameter can be determined via different relationships reported across the open literature; however, each are directly related to the ratio of the liquid and vapor mass flow rates (L/V, –) through the column.[98,123] We use reported column diameter calculations and correlations for both random and structured packing materials summarized in Seader, Henly, and Roper.[98] A commonly used liquid-gas kinetic energy factor, F_{LV} (–), establishes a relationship between the liquid phase mass flow rate (L (kg s^{-1})), liquid molecular weight (M_L (g mol^{-1})), liquid phase density (ρ_L (kg m^{-3})), gas phase mass flow

rate (V (kg s^{-1})), gas molecular weight (M_G (g mol^{-1})), and gas phase density (ρ_G (kg m^{-3})) as shown in **Eq. 22**.

$$F_{LV} = \left(\frac{LM_L}{VM_G}\right)\left(\frac{\rho_G}{\rho_L}\right)^{0.5} \quad (22)$$

The vapor flow rates are set by the flue gas stream emitted from the power plant or industrial facility, while liquid flow rates require additional design decisions. It has been observed that as long as $0.005 < F_{LV} < 5$ for random packing materials and $0.005 < F_{LV} < 2$ for structured packing, an absorption column can maintain sufficient flooding and pressure drop conditions.[123,124] Given this range and the relationship described in **Eq. 22**, for a 17.45% CO_2 flue gas stream with a density of 1.32 m^3 kg^{-1} (N_2 difference at 1 bar and 20°C) and a liquid solution with a density of ~1000 m^3 kg^{-1}, the absorber can successfully perform the desired separation with L/V ratios ranging from ~0.5 to ~110.[98] Despite the wide operating window, prior cost optimizations have suggested that MEA-based capture systems should operate around $L/V \approx$ 1.4-2.5 to minimize the thermal energy required to release CO_2 and regenerate the sorbent.[125] Thus, while the absorber can operate at a range of flow rates, process optimization may be required to understand the effects of altered flow rates on the efficiency of adjacent units.

Experimental data collected at constant pressure drop column flooding conditions have been used to develop isobaric trends / correlations between the independent variable, F_{LV}, and an empirical factor, F_C (–), which is a function of the vapor velocity, packing factor, liquid phase density, gas phase density, and liquid kinematic viscosity.[126,127] Its expression is expanded in **Eq. S1**. The pressure drop at flooding conditions can be calculated from the packing material packing factor (**Eq. S2**), enabling the determination of F_C via interpolation across the lines of constant pressure drop in the correlations discussed above.[98] From F_C, it is possible to calculate the superficial vapor velocity, $u_{G,flood}$ (m s^{-1}), and calculate the column diameter, D_{abs} (m), via **Eq. 23**.[98]

$$D_{abs} = \left[\frac{4V}{f u_{G,flood} \pi \rho_G}\right]^{0.5} \quad (23)$$

Where ρ_G (kg m^{-3}) is the gas phase density, $u_{G,flood}$ (m s^{-1}) is the estimated gas phase flooding velocity, and f (–) is the fraction of flooding in the column. This flooding fraction can vary, but typical absorbers operate between 0.5 and 0.7.[123] While Towler and Sinott recommend that the column be designed to operate at the highest economical pressure drop, this is left for future techno-economic optimization and, in this work, we simply focus on maintaining good liquid and gas distributions by keeping F_{LV} within the acceptable range and allowing the pressure drop to vary accordingly.[123] Further details regarding this calculation are included in the **Section S.4.1** of the **SI**.

3.2. Absorption Column Sizing Model: Height

To determine the absorber height, we assume thermal equilibrium across the gas and liquid phases, isothermal behavior in the column, ideal gas behavior, counter current flow through the column, and that plug flow applies to both the gas and liquid phases through the bulk of the column, as is typically assumed in such models.[117,118,128–133] Additionally, we assume that CO_2 is the only species transferred across the interface and that we can represent the fluxes across this gas/liquid interface in a two-film model.[118,128,129,131] While we apply a plug flow assumption here, it is important to note that axial mixing may become important at industrial scales.[134–137] To verify that the plug flow assumption is valid, we can use the largest calculated axial dispersion coefficient, ~2.87 × 10^{-3} m^2 s^{-1},[128] from a reactive absorption pilot plant (similar in size to the columns we contemplate in this work) as well as process-relevant gas velocities and packing material particle diameters in order to calculate the Bodenstein number $\left(Bo = \frac{u_G d_p}{\mathcal{D}_{ax}}\right)$, where u_G (m s^{-1}) is the gas velocity, d_p (m) is the packing material diameter, and $\mathcal{D}_{ax}$ (m^2 s^{-1}) is the axial dispersion coefficient.[128] The Bo number is used to determine if dispersion is significant by comparing the amount of species introduced by convection to that introduced by dispersion, such that high values approach plug flow conditions with no back-mixing (convection dominates) while low values approach stirred tank-reactor conditions and exhibit full back-mixing (dispersion/diffusion dominates).[138] We observe that under conditions relevant to this work, $Bo \gg 1$, suggesting that convection effects are more important than dispersion effects.[128,136] In

general, the effects of dispersion would reduce the mass transfer driving forces, thus leading to an underestimation of column height under the plug flow assumption.[136]

To determine the column height, we model the concentration profiles and partial pressures of all reacting species from the bottom to the top of the unit. The outlet stream concentrations are calculated using the material balances outlined in **Section 2.2** and **Section 2.3**. Using the CO_2 partial pressure profile, we determine the height at which the desired capture fraction is achieved. Accordingly, we develop the following set of index 1 differential algebraic equations (DAEs) for both direct and indirect eCCC as has been previously done for isothermal reactive absorption models to solve for the gas-phase molar flow rate and concentration profiles along the column height.[117,120] The gas-phase continuity equation for the CO_2 that is absorbed by the liquid along the height, z (m), is displayed as **Eq. 24**:

$$\frac{dP_{CO_2}}{dz} = \frac{A}{\bar{V}}\left(P_0 a_w N_{CO_2}\big|_{y=0}\right) \tag{24}$$

where P_{CO_2} (bar) is the partial pressure of CO_2 in the gas stream, A (m^2) is the cross-sectional area of the column, $\bar{V}$ (mol h^{-1}) is the total molar flow rate of the vapor stream, P_0 (bar) is the total pressure, a_w (m_I^2 $m_{packing}^{-3}$) is the effective interfacial area of packing per unit packed volume, and $N_{CO_2}\big|_{y=0}$ (kmol m_I^{-2} h^{-1}) is the flux of CO_2 across the gas-liquid interface that can be calculated from the two-film model (*vide infra*).

The liquid-phase continuity equation for the CO_2 that is absorbed from the gas and further reacted either with the redox-active sorbent (R) in the case of direct capture processes or with the hydroxides (OH^-) in the case of indirect capture processes can be written as **Eq. 25**:

$$\frac{d[CO_2]}{dz} = \frac{A}{\dot{Q}_L}\left(a_w N_{CO_2}\big|_{y=\delta} - r_1 h_L\right) \tag{25}$$

where $[CO_2]$ (kmol m_L^{-3}) is the concentration of dissolved CO_2 in the liquid, $\dot{Q}_L$ (m_L^3 h^{-1}) is the liquid volumetric flow rate (a constant value), $N_{CO_2}\big|_{y=\delta}$ (kmol m_I^{-2} h^{-1}) is the flux of CO_2 leaving the liquid boundary layer (*vide infra*), δ (m) is the liquid boundary layer thickness, r_1 (kmol m_L^{-3} h^{-1}) is the rate of CO_2 reaction in the liquid, and h_L (m_L^3 $m_{packing}^{-3}$) is the liquid hold-up (*vide infra*).

To account for changes in the molar flow rate of the gas phase throughout the absorption column we apply **Eq. 26**:

$$\frac{d\bar{V}}{dz} = a_w N_{CO_2}\big|_{y=0} A \tag{26}$$

The final universal algebraic expression for modeling CO_2 absorption in direct and indirect eCCC describes the CO_2 balance around the bottom of the column (**Eq. 27**):

$$\dot{Q}_L(\mathrm{DIC}_z) + \bar{V}_1 y_{1,CO_2} = \dot{Q}_L(\mathrm{DIC}_2) + \bar{V}_z y_{z,CO_2} \tag{27}$$

where the subscripts 1 and 2 refer to the conditions in Stream 1 and Stream 2, respectively, and subscript z refers to the values at a particular column height.

Beyond these general absorption column relationships that apply to all systems, there are further equilibrium expressions and balances, outlined in **Table 1**, that need to be applied specifically to direct or indirect eCCC processes. In addition to tracking the CO_2 partial pressure and the gas flow rate, we must account for 5 species in solution in the direct capture process (CO_2, R^{n-}, $R(CO_2)_q^{n-}$, R, and $R(CO_2)$) while the indirect capture process involves 8 solubilized species (CO_2, HCO_3^-, CO_3^{2-}, OH^-, H^+, Q^{2-}, QH^-, and QH_2). The additional 3 species in the indirect process necessitate further expressions to fully define the index 1 DAE.

Table 1. Additional equilibrium expressions and material balances for the direct and indirect eCCC processes that are applied to solving for the absorption column height. In these expressions, $[i]$ (kmol m^{-3}) represents the concentration of species i in the liquid phase at height z (m), $[R_{tot}]$ (kmol m^{-3}) is the total concentration of capture species R in solution (in all oxidation states), $[Q_{tot}]$ (kmol m^{-3}) is the total concentration of mediator species Q in solution (in all oxidation states), subscript z represents height z (m), and a subscript of 2 in reference to concentrations (i.e., not the equilibrium expressions) represents the value at the liquid outlet Stream 2.

	Direct	**Indirect**
1	$K_{2,direct} = \frac{[\mathrm{R(CO_2)}][C_0]}{[\mathrm{R}][\mathrm{CO_2}]}$	$K_{2,indirect} = \frac{[\mathrm{CO_3^{2-}}][\mathrm{H^+}]}{[\mathrm{HCO_3^-}][C_0]}$
2	$\left(0.5 + \frac{\Delta x_a}{2}\right)[R_{tot}] = [\mathrm{R(CO_2)_q^{n-}}] + [\mathrm{R^{n-}}]$ (total activated capture species balance)	$K_w = \frac{[\mathrm{H^+}][\mathrm{OH^-}]}{[C_0]^2}$

3	$\left(0.5-\frac{\Delta x_a}{2}\right)[R_{tot}]=[\mathrm{R(CO_2)}]+[\mathrm{R}]$ (total deactivated capture species balance)	$K_{a,1}=\frac{[\mathrm{QH^-}][\mathrm{H^+}]}{[\mathrm{QH_2}][C_0]}$
4		$K_{a,2}=\frac{[\mathrm{Q^{2-}}][\mathrm{H^+}]}{[\mathrm{QH^-}][C_0]}$
5		$\mathrm{TA}_z=\mathrm{TA}_2$ (total alkalinity / charge balance)
6		$\left(0.5+\frac{\Delta x_a}{2}\right)=\frac{[\mathrm{Q^{2-}}]+[\mathrm{QH^-}]+[\mathrm{QH_2}]}{[\mathrm{Q}_{tot}]}$ (total reduced mediator species balance)

In the above differential equations, the effective interfacial area, a_w (m^2 m^{-3}), for random packing materials has been empirically studied and can be determined through Onda's correlations using the actual interfacial area of packing per unit packed volume (a, m^2 m^{-3}) and other fluid physicochemical properties.[139] This is outlined in **Section S.4.2** of the **SI**. For structured packing, we implement correlations developed by Hanley and Chen, as outlined in **Section S.4.3** of the **SI**.[140] Additionally, the definition of the liquid hold-up, h_L, uses the dimensionless expression developed by Billet and Shultes that is outlined in **Section S.4.4** of the **SI**.[98,141]

3.3. Two-Film Model

The flux across the interface $\left(N_{CO_2}\big|_{y=0}\right)$ and the liquid boundary layer $\left(N_{CO_2}\big|_{y=\delta}\right)$ used in the above plug flow model can be determined from a two-film model developed for the direct and indirect capture processes. While several models exist that describe this interfacial behavior (i.e., two-film, penetration, or surface renewal theory),[120,121] we choose the two-film approach to simplify our model while still capturing the uncertainty in the electrochemical system reaction rates and mechanisms. In the gas phase, we assume that the resistance to mass transfer is related to Henry's law:

$$[\mathrm{CO_2}]_{I,z}=H_{CO_2}P_{CO_2,z} \tag{28}$$

where $[CO_2]_{I,z}$ (kmol m^{-3}) is the concentration of CO_2 in the liquid at the gas-liquid interface (I) for a given column height (z), H_{CO_2} (kmol m^{-3} bar^{-1}) is the Henry's law constant for CO_2, and $P_{CO_2,z}$(bar) is the partial pressure of CO_2 in the gas phase at a given column height (z). For the boundary layer in the liquid phase, we model the resistance to mass transfer via a reaction-diffusion framework based on the following steady-state expression:

$$0 = \mathcal{D}_i \frac{d^2[i]}{dy^2} + r_i \tag{29}$$

where y (m) is the distance from the interface in the liquid-phase reaction boundary layer, $\mathcal{D}_i$ (m^2 s^{-1}) is the diffusion coefficient of species i, and the reaction term, r_i (kmol m^{-3} s^{-1}), is the rate of consumption of species i.

Direct Capture Two-Film Model

We first derive the set of equations for the boundary value problem in a direct eCCC process by expressing each of the unknown species boundary layer concentrations ($[CO_2]$, $[R^{n-}]$, $[R(CO_2)^{n-}]$, [R], and $[R(CO_2)]$) in a set of differential equations. In accordance with **Eq. 3** and **Eq. 5**, there are two possible reactions that can occur in the direct eCCC column, and their rate laws can be represented by the following expressions:

$$r_{1,direct} = -k_{1,f,direct}\left([CO_2][R^{n-}] - \frac{[R(CO_2)^{n-}][C_0]}{K_{1,direct}}\right) \tag{30}$$

$$r_{2,direct} = -k_{2,f,direct}\left([CO_2][R] - \frac{[R(CO_2)][C_0]}{K_{2,direct}}\right) \tag{31}$$

where $r_{1,direct}$ and $r_{2,direct}$ (kmol m^{-3} s^{-1}) are the rates of the two CO_2 absorption/ desorption reactions and $k_{1,f,direct}$ and $k_{2,f,direct}$ (m^3 kmol^{-1} s^{-1}) are the forward rate constants for those reactions. **Eq. 30** and **Eq. 31** are written in terms of their forward rate constants and the equilibrium expressions.

As with the material balances across the column, we assume that the reaction between CO_2 and the deactivated capture species (R) is in equilibrium, and thus $r_{2,direct} = 0$, eliminating the dependence of $[CO_2]$ on [R] and $[R(CO_2)]$ in the thin film. Thus, for the direct capture process, we do not monitor the

concentrations of the deactivated capture species in the film as this is not required to calculate the CO_2 flux through the boundary layers and across the interface. Additionally, while this process will require counter ions in the form of a supporting electrolyte, they are not directly involved in the equilibria and are assumed to be present in excess in solution. Thus, they can be ignored in this analysis. In accordance with **Eq. 29** and **Eq. 30**, we write the following differential equation describing the concentration profile of CO_2 through the liquid film.

$$r_{1,direct} = -\mathcal{D}_{CO_2}\frac{d^2[\mathrm{CO_2}]}{dy^2} = -k_{1,f,direct}\left([\mathrm{CO_2}][\mathrm{R}^{n-}] - \frac{[\mathrm{R(CO_2)}^{n-}][C_0]}{K_{1,direct}}\right) \tag{32}$$

Similar expressions can be developed for $[\mathrm{R}^{n-}]$ and $[\mathrm{R(CO_2)}^{n-}]$ as outlined in **Section S.5** of the **SI**. At the gas-liquid interface ($y = 0$), we define Neumann boundary conditions to set the flux of R^{n-} and $\mathrm{R(CO_2)}^{n-}$ equal to 0 since we assume that the capture species cannot leave the liquid phase. At this interface, we also set the flux of CO_2 in the gas and liquid phases equal. In the gas film, the rate of mass transfer and thus the flux can be expressed in terms of k_G (kmol m^2 s^{-1} bar^{-1}), the mass-transfer coefficient in the gas phase.

$$N_{CO_2}\big|_{y=0} = k_G\left[P_{CO_2,b} - P_{CO_2,I}\right] \tag{33}$$

This can be related to the liquid phase via:

$$k_G\left[P_{CO_2,b} - P_{CO_2,I}\right] = -\mathcal{D}_{CO_2}\frac{d[\mathrm{CO_2}]}{dy}\bigg|_{y=0} \tag{34}$$

where subscript b and I refer to the bulk and interfacial values, respectively. $P_{CO_2,I}$ is determined from the calculated interfacial concentration in the liquid (**Eq. 28**), as we assume that there is no resistance to mass transfer at the interface ($y = 0$). The value of the gas-phase mass-transfer coefficient, k_G, is calculated from system properties using the correlations developed by Onda et al.[139] for random packing materials (or Hanley and Chen[140] for structured packing) as outlined in the **Sections S.4.2** and **S.4.3** of the **SI**. The final boundary conditions at $y = \delta$ require that all concentrations in the liquid film equal those in the bulk solution.

To address the uncertainty in capture species properties and to simplify the numerical solution to this boundary value problem, we elect to non-dimensionalize the preceding framework. As was mentioned in **Section 2.2**, direct eCCC is a nascent concept and thus detailed analyses of archetypal species are scant. Consequently, important parameters such as $k_{1,f,direct}$ and capture species diffusion coefficients ($\mathcal{D}_{R^{n-}}$ and $\mathcal{D}_{R(CO_2)^{n-}}$) remain unknown, but the impact of their relative scales can be understood through dimensional analysis. While these variables are unknown in the context of eCCC, their magnitudes can be estimated through a compilation of similar molecules in adjacent electrochemical systems (e.g., redox flow batteries (RFBs)). Consequently, we choose to define a key dimensionless group, the Damköhler number $\left(Da = \frac{(k_{1,f,direct})\delta^2[\mathrm{R_{tot}}]}{\mathcal{D}_{R^{n-}}}\right)$, that relates the chemical reaction rate to the rate of transport in the solution. To simplify the analysis further, we also assume that $\mathcal{D}_{R^{n-}} = \mathcal{D}_{R(CO_2)^{n-}}$; however, it is likely that once CO_2 is bound to the capture species, the diffusion coefficient will be lowered, reducing the rate of transport. Additionally, we can calculate the value of the boundary layer thickness, δ (m), from the liquid-phase mass transfer coefficient, k_L (m s^{-1}), via $k_L = \frac{\mathcal{D}_{CO_2,l}}{\delta}$, where k_L can be determined from the Onda[139] and/or Hanley/Chen[140] correlations shown in **Sections S.4.2** and **S.4.3** of the **SI**.[98] The final dimensionless differential equations used in the model for all three species are derived in **Section S.5** of the **SI**.

Indirect Capture Two-Film Model

For the indirect capture process, we consider several different reactions that must be accounted for in the liquid electrolyte. According to **Eq. 11** – **15**, there are 5 possible reactions/equilibria that occur in the absorber:

$$r_{1,indirect} = -k_{1,f,indirect}[\mathrm{CO_2}][\mathrm{OH^-}] \tag{35}$$

$$r_{2,indirect} = -k_{2,f,indirect}\left([\mathrm{HCO_3^-}] - \frac{[\mathrm{H^+}][\mathrm{CO_3^{2-}}]}{K_{2,indirect}[C_0]}\right) \tag{36}$$

$$r_w = k_{w,f}\left(\frac{[\mathrm{H^+}][\mathrm{OH^-}]}{K_w[C_0]^2}\right) \tag{37}$$

$$r_{Q,1} = -k_{Q,1,f}\left([\mathrm{QH_2}] - \frac{[\mathrm{H^+}][\mathrm{QH^-}]}{K_{a,1}[C_0]}\right) \quad (38)$$

$$r_{Q,2} = -k_{Q,2,f}\left([\mathrm{QH^-}] - \frac{[\mathrm{H^+}][\mathrm{Q^{2-}}]}{K_{a,2}[C_0]}\right) \quad (39)$$

where each of the reaction rates (r (kmol m^{-3} s^{-1})) are related to the rate constants ($k_{1,f,indirect}$, $k_{2,f,indirect}$, $k_{w,f}$, $k_{Q,1,f}$, and $k_{Q,2,f}$) via their studied rate laws. **Eq. 35** – **Eq. 39** are all written in terms of their forward rate constants and the equilibrium expressions. In the indirect eCCC column, we assume that only the out-of-equilibrium reaction is that described by **Eq. 35**. Given the larger number of species in solution, additional equilibrium expressions to consider (K_w, $K_{2,indirect}$, $K_{a,1}$, and $K_{a,2}$), and the presence of counter ions that are involved in the equilibrium expressions (i.e., protons), a slightly different set of expressions are developed as compared to those for the direct eCCC.

As with the direct eCCC process, we can write a system of differential equations for all 8 species; however, because there are 4 equilibrium expressions, we only need to solve 4 differential equations. The relevant differential equations for the indirect capture reactions are outlined in the **Eq. S13** – **Eq. S20** in the **SI**. Like the direct capture process, we can extract the CO_2 reaction term and differential equation by combining **Eq. 13** and **Eq. 35**:

$$r_{CO_2} = -\mathcal{D}_{CO_2}\frac{d^2[\mathrm{CO_2}]}{dy^2} = -k_{1,f,indirect}[\mathrm{CO_2}][\mathrm{OH^-}] \quad (40)$$

A key difference between the direct and indirect capture processes stems from the availability of a TA balance or charge balance. Employing this balance along with a DIC balance and a reduced mediator species balance results in the following three differential equations that, when coupled with the equilibrium expressions and the CO_2 reaction term above, can be solved for all species concentration profiles in the boundary layer.

$$-\mathcal{D}_{HCO_3^-}\frac{d^2[\mathrm{HCO_3^-}]}{dy^2} - 2\mathcal{D}_{CO_3^{2-}}\frac{d^2[\mathrm{CO_3^{2-}}]}{dy^2} - \mathcal{D}_{OH^-}\frac{d^2[\mathrm{OH^-}]}{dy^2} - 2\mathcal{D}_{Q^{2-}}\frac{d^2[\mathrm{Q^{2-}}]}{dy^2} - \mathcal{D}_{QH^-}\frac{d^2[\mathrm{QH^-}]}{dy^2} + \mathcal{D}_{H^+}\frac{d^2[\mathrm{H^+}]}{dy^2} = 0 \quad (41)$$

$$-\mathcal{D}_{CO_2}\frac{d^2[\mathrm{CO_2}]}{dy^2}-\mathcal{D}_{HCO_3^-}\frac{d^2[\mathrm{HCO_3^-}]}{dy^2}-\mathcal{D}_{CO_3^{2-}}\frac{d^2[\mathrm{CO_3^{2-}}]}{dy^2}=0 \quad (42)$$

$$-\mathcal{D}_{QH_2}\frac{d^2[\mathrm{QH_2}]}{dy^2}-\mathcal{D}_{QH^-}\frac{d^2[\mathrm{QH^-}]}{dy^2}-\mathcal{D}_{Q^{2-}}\frac{d^2[\mathrm{Q^{2-}}]}{dy^2}=0 \quad (43)$$

Employing these expressions allows us to balance charge in the system while minimizing the number of forward rate constants required to perform the calculations. The full derivation of these differential equations and further non-dimensionalization for use in a numerical solver are described in **Section S.6** of the **SI**.

Numerical Solutions

For the entirety of this model, we used MATLAB® R2023a on a Dell Latitude 7300 laptop computer with an Intel® Core™ i7-8665U processor (quad core, 1.90 GHz) and 16 GB of random-access memory. With each iteration over the height of the absorption column, the two-film model is simultaneously solved to determine the flux of CO_2 across the gas-liquid interface and into the bulk liquid. Each of these sets of differential equations are solved within the absorption column DAE using either MATLAB's *bvp4c* function (direct capture process) or a central, second-order finite differencing scheme (indirect capture process). While the direct capture process produced the same results using *bvp4c* as were achieved using a finite differencing scheme, we chose to utilize the simple transition to *bvp4c* to reduce the computation time. Given the interdependence and number of differential expressions within the indirect eCCC model (**Eq. 40** – **Eq. 43**), input into the MATLAB function *bvp4c* would require a reformulation of the equations and thus was not pursued at this time. The direct and indirect capture baseline models solve for the column size in 31.08 s and 34.93 s, respectively.

4. Results and Discussion

Given the similar CO_2 capture targets expected of electrochemical and thermochemical systems, we aim to directly compare absorption column sizes to assess if eCCC can either exploit smaller columns or eventually act as retrofitted replacements to existing amine platforms. Accordingly, using the outlined

framework and inlet flue gas concentrations obtained from a studied amine-capture pilot plant facility, we calculate the required size of an eCCC absorption column to achieve the same capture efficiency. We first validate the model using well-studied thermochemical systems (**Section 4.1**), then using a pilot plant from the validation section, we investigate the column sizes that would enable the direct (**Section 4.2**) and indirect (**Section 4.3**) eCCC processes to remove the same amount of CO_2 from the same flue gas stream. Lastly, we investigate the impact that select molecular properties and operating conditions have on the column volume and assess the feasibility of designing eCCC absorbers that are comparable in size or smaller than those in current amine-based systems (**Section 4.5**).

4.1. Model Validation

To assess the accuracy of our model, we use data collected from experimental and pilot plant studies performed for CO_2 capture via MEA sorbents. Unlike eCCC, capture via amine-based absorbents is well-studied, with physical properties, reaction rates, and experimental conditions widely available. While the absorption mechanism is like that of direct eCCC (i.e., the amine binds with CO_2 directly), the overall reaction between MEA and CO_2 is represented as follows:

$$2\mathrm{RNH_2} + \mathrm{CO_2} \xrightarrow{k_{1,f,MEA}} \mathrm{RNHCOO^-} + \mathrm{RNH_3^+} \tag{44}$$

where "R" for MEA represents CH_2CH_2OH and $k_{1,f,MEA}$ (m^3 $kmol^{-1}$ s^{-1}) is the forward, second-order rate constant for the amine capture.

For this validation, we choose to only investigate MEA-based systems (rather than other alkanolamine systems) because the reaction kinetics are second-order with respect to MEA and CO_2, which aligns with our assumption for the direct eCCC reaction kinetics.[26,94,95] Various correlations between $k_{1,f,MEA}$ and temperature have been reported across the peer-reviewed literature,[94,95,142] but for validation, we choose to follow the Versteeg kinetic expression (**Table S2** in the **SI**).[95] To incorporate $k_{1,f,MEA}$ into the absorption column model, we calculate the Da from this rate constant, the liquid-phase mass transfer coefficient (k_L,

as described in **Section S.4.2** and **Section S.4.3** in the **SI**), the species concentration, and the diffusion coefficient of MEA in water. For the MEA system, because we are assuming an irreversible reaction at a large equilibrium constant,[26,94,95] the formation of two, stoichiometrically equivalent molecular species does not require any additional expressions in the thermochemical absorber model. However, we do alter the stoichiometric coefficients in accordance with the overall reaction.

Additional liquid properties (i.e., the diffusivity of CO_2 ($\mathcal{D}_{CO_2,L}$), diffusivity of MEA (equivalent to $\mathcal{D}_{R,L}$ from eCCC), viscosity (μ_L), density (ρ_L), molecular weight (M_L), surface tension (σ_L), and Henry's constant for CO_2 (H_{CO_2})) were estimated via a combination of established correlations and reported data in prior literature. The values/correlations selected are detailed in **Table S2** in the **SI**. Because the flue gas inlet is maintained across the thermochemical and electrochemical systems, the gas stream properties are all the same and are identified in **Table S4** in the **SI**.

To initially assess the ability for our model to accurately determine the column inlet / outlet gas and liquid compositions, as well as predict concentration profiles, we use model results from De Leye and Froment[117] where all species compositions (i.e., solution-phase reactant concentrations, solution-phase product concentrations, and gas-phase CO_2 partial pressures) were reported along the column length, enabling full model validation. The findings from this validation are shown in **Figure 3Error! Reference source not found.a**. In the middle of the column, it appears as though our model underpredicts the partial pressure of CO_2 in the gas phase (suggesting a faster rate of CO_2 absorption in our model), however, this apparent discrepancy may be attributed to two key differences: 1) we assume that the volumetric flow rate of the solution through the column remains constant while De Leye and Froment allow this to vary and 2) we fully model the kinetic relationships in solution rather than using enhancement factors and Hatta numbers to calculate CO_2 flux across phases.[117] Specifically, we observe that our assumption regarding a constant volumetric flow rate of the solution through the column leads to concentrations of RNH_2 and the two product species at the bottom of the column that are slightly greater than those reported by De Leye

and Froment ([RNH_2] = 0.455 M and [$RNHCOO^-$] = 0.882 M in our model while [RNH_2] = 0.435 M and [$RNHCOO^-$] = 0.852 M in De Leye and Froment). When this assumption is relaxed and flow rates are allowed to vary, our model generates outputs of [RNH_2] = 0.438 M and [$RNHCOO^-$] = 0.850 M, which are near-identical to those reported previously, explaining the difference in concentrations along the column length. While not validated explicitly, it is still possible that the final, small difference in composition may be attributed to the kinetic formulation/correlations selected.

To quantitatively assess the validity of the concentration profiles predicted in our model, we use the R^2 metric (**Eq. 4.2**).

$$R^2 = 1 - \frac{SSR}{SST} = 1 - \frac{\sum_z \left(y_{CO_2,z,\text{lit}} - y_{CO_2,z,\text{pred.}}\right)^2}{\sum_z \left(y_{CO_2,z,\text{lit}} - \bar{y}_{CO_2,\text{lit}}\right)^2} \tag{4.2}$$

Where *SSR* is the sum of square residuals, *SST* is the total sum of squares, $y_{CO_2,z,\text{lit}}$ is the mole fraction of CO_2 in the gas stream at height z reported in literature, $\bar{y}_{CO_2,\text{lit}}$ is the column averaged mole fraction of CO_2 in the gas phase as reported in literature, and $y_{CO_2,z,\text{pred.}}$ is the mole fraction of gaseous CO_2 predicted in our model at the same column height as that reported in literature. The R^2 value for the model fit to the De Leye and Froment CO_2 partial pressure profile is 0.97, suggesting reasonable agreement. Furthermore, the height reported in this prior model was 11 m while our model predicts a height of 9.1 m, a 17.3% error. A potential cause of these differences is discussed below.

While De Leye and Froment offer a reasonable validation framework for tracking species concentrations in the liquid phase, we further compare our model to four other experimental plant-, pilot-plant-, and bench-scale MEA absorption columns. These columns include a pilot-plant-scale column reported by Dugas to separate CO_2 from flue gas in a study at The University of Texas at Austin (Run 32),[112] an industrial-scale absorption column that reduced CO_2 content from a natural gas stream (Run 106),[113] a small-scale pilot plant reported by Tontiwachwuthikul et al. designed to monitor concentrations across the length of the column (Run T22),[143] and a column used for bench-scale laboratory experiments reported by

DeMontigny et al. (Run 7).[114] The experimental conditions for each of the studies are outlined in **Table S5** in the **SI**. Three of the columns (Runs 32, 106, and T22) contained random packing materials whereas the fourth (Run 7) contained structured packing. Experimentally determined concentration profiles along the column lengths are often less accessible, potentially due to the difficulty in monitoring column internals. As a result, sample data points may be limited to the inlet and outlet CO_2 mole fractions in the gas phase. Nevertheless, in some instances, these experimental studies have been supported by first-principles models, which can predict actual column performance that aligns with available experimental information.[96,144,145]

Combining the reported experimental and modeling data (when available), we validated the accuracy of our model in calculating column heights and concentration profiles. We find that the predicted error in heights vary widely, with the most accurate underestimating the height by only 2.12% (Run 32) while the least accurate overestimated the height by 36.6% (Run 7) (**Figure 3b**). Although this error may seem large, we observed that the column height is highly sensitive to capture fractions exceeding 99%, as changing the value by tenths of a percent above this threshold significantly altered the final estimated height. This phenomenon arises from the inherent challenge of separating such small concentrations of CO_2 at elevated capture fractions. Further, the introduction of computational error at the low CO_2 partial pressures measured at the top of the column is likely to complicate the height prediction. To support these assertions, we note that three out of the four columns studied reported capture fractions >99% (i.e., Run 106, Run T22, and Run 7 were reported to achieve capture fractions of 99.92%, 99.99% and ~100%, respectively). In **Figure 3b**, we note that each of the heights calculated for these scenarios deviate significantly from their reported values (i.e., relative errors ≥ 9.9%); however, when we lower the percent captured from ~100% (99.9999%) to 99.99% for Run 7, the error in the height changes from an overestimate of 36.61% to an underestimate of 8.11%, exemplifying the extreme sensitivity to high capture fractions. The column used in Run 7 was also a relatively small, experimental apparatus (2.16 m in height), thus the error in the height calculation may be exacerbated by small changes in height. Taken together, the effects of high capture fractions and short columns suggest that the relative errors are likely not indicative of model inaccuracy.

Next, we assess the R^2 values for our model as compared to the experimental columns. There are two possible R^2 values that can be utilized. The first aligns with that which was previously calculated, where we compare the gaseous CO_2 concentrations between our model and the prior models reported in literature. This method allows us to have many data points upon which R^2 can be evaluated. The second method to calculate R^2 comes from comparing our model results to any experimental data points. A key limitation of this method is that in some experiments (i.e., Run 32 and Run 106), there are only two available data points—one at the inlet and one at the outlet of the gas stream in the column. In these cases, if our model underpredicts the height, we cannot compare the CO_2 concentrations exactly at the "outlet" of the experimental column. Thus, for the purposes of determining the model accuracy against experimental reports, we permit our model to report CO_2 concentrations beyond the desired capture fraction (i.e., our model captures more CO_2 than the experiment) such that the exact CO_2 concentration at the height of the experimental column can be estimated. The resulting R^2 values from both methods are outlined in **Figure 3c**, where the darker color bars signify the R^2 values for any available model comparisons, while the lighter colors signify R^2 values for any available experimental comparisons. The R^2 values for the model comparisons range from 0.90 to 0.99, while the R^2 values for experimental comparisons range from 0.86 to 0.99. Available models for Run 32 investigate column temperature profiles[25,118,124] or perform dynamic analyses,[118,146] but, to the best of our knowledge, no relevant profiles for CO_2 concentration in the gas stream were reported. While Afkhamipour et al. do model the CO_2 concentration profiles for Run 32, they use the total column height (including sections without packing) while we only investigate the 6.1 m of packed materials to ensure mass transfer coefficients apply across the entire domain simulated.[96] For the runs with several experimental data points taken from inside of the column (i.e., Runs T22 and 7), we observe that the R^2 values differ slightly between the model and experimental comparisons, as Run T22 achieves R^2 = 0.904 in the model comparisons and R^2 = 0.858 for experimental comparisons, whereas Run 7 achieves R^2 = 0.914 in the model comparisons and R^2 = 0.957 in the experimental comparisons. The substantial disparities in the R^2 values for Run T22 suggest that our model aligns well with other reactive absorption

models of randomly packed columns, but when compared to the experimental data, the accuracy of the fit diminishes. The deviations between our model and experimental data may be due to the constant temperature assumption, as exothermic reactions, heat transfer between phases, and heat loss along the column walls can change the operating temperature, affecting the rate of reaction and, consequently, the CO_2 profiles.[38] However, given the high R^2 values generated, such effects are unlikely to impact the general findings and trends reported here. To generally quantify the magnitude of the error introduced by assuming isothermal operation, we used available temperature profiles along the length of the column in Run 32 to evaluate the predicted column height if the temperature were set at the minimum (41.3 °C) or maximum (64.3 °C) values. At 41.3 °C, the calculated column height is 6.36 m, while at 64.3 °C, the column height is lowered to 5.23 m. The column is shorter at elevated temperatures due to the faster CO_2 uptake reaction rates. Given that the experimental column height is 6.1 m, by assuming isothermal operation it is possible that our model can overestimate the height by 4.3% or underestimate it by 14.26%. These set the upper bounds on the error introduced due to temperatures in Run 32, but it is likely that similar trends will result across other thermochemical columns.

On the contrary, while Run 7 also exhibits slightly different R^2 values between experimental and modeling data, a comparison of the CO_2 gas phase concentration profiles from our model and the profiles reported in literature shows that our results fall in between prior experimental and modeling data points (**Figure S3d** in the **SI**). The high R^2 values observed for the four columns coupled with the strong qualitative agreement observed in **Figure S3** in the **SI** evince reasonable alignment between our model and prior literature, suggesting that we are capturing absorption column dynamics to a reasonable degree and this framework can be useful for exploring eCCC.

In addition to height validation, it is also possible to compare calculated mass transport coefficients in the liquid and gas phases of the column. A discussion of this validation step is expanded on in **Section S.8.** of the **SI**, and **Figures S4** and **S5** display comparisons between the values computed in our model and those

in the experimental columns. We observe that, generally, the values we compute for mass transfer coefficients in both phases are comparable to those calculated in prior works.

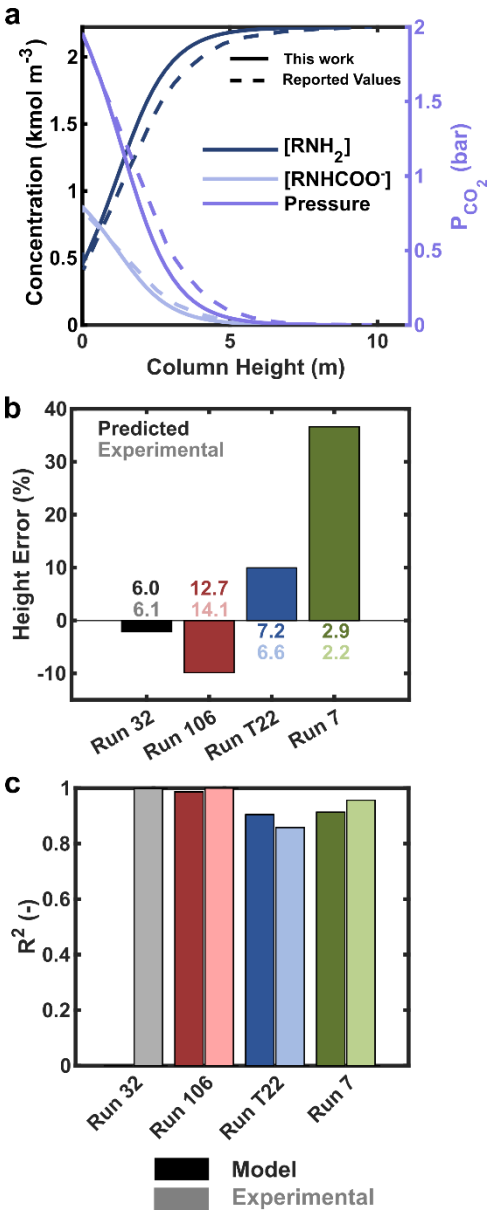

Figure 3. (a) Concentration validation against the prior model reported in De Leye and Froment, where the bottom of the column is set to 0 m.[117] The dashed lines represent reported values for the column while the solid lines represent results from our model. (b) Percent error in the absorption column height predictions, the numbers above and below the bars represent column heights (m) predicted in this work (dark color) and reported from experimental studies (light colors). (c) R^2 values from modeling performed in this work vs. both the models previously developed (dark columns) and any experimental data collected (light columns) to investigate the relative extents of agreement.

While using the reported MEA physical fluid properties (i.e., diffusion coefficients, viscosities, densities, temperature, total pressure, etc.) results in sufficient model validation, we also conducted a brief sensitivity analysis to explore the effects of varying these properties on column height estimates. Given that these properties are not yet well-defined for the electrochemistries intended for carbon capture, it is important to understand their impact on our model. The changes in the calculated column height that result from changing these species properties by ±10% are presented in **Figure S6** in the **SI** for Run 32 (the study with the most accurate column height). At most, we observe that the height changes by only ±5.8%, suggesting that for the electrochemical systems modeled in this work, minor sizing errors may result even if we apply reasonable property estimates based on the expected solvents and active species.

For all further comparisons presented in this work, we use the pilot plant described by Dugas (Run 32).[112] We selected this as our model system because the experimental results from this pilot plant are extensively referenced across thermochemical capture literature[8,37,124,145–150] and our model most accurately predicts the column height while maintaining strong agreement with reported experimental data points. The lower, yet more common, 95% capture fraction likely enables accurate column sizing while also allowing us to align our model with traditional PCC capture fraction goals.[20]

Beyond the height, we must ensure that our model can accurately calculate the column diameter used in the experiment. As discussed in **Section 3.1**, the diameter is dependent on the liquid and gas stream flow rates, fluid properties (i.e., stream densities, viscosities, molecular weights, etc.), packing properties, and flooding fraction. The flooding fraction for Run 32 was not reported in the original work by Dugas,[112] thus we use the known diameter for the study to back-calculate the flooding fraction via **Equation 23**. At the reported conditions and with a column diameter of 0.427 m, we estimate the flooding fraction as 0.27. While this value falls below the typical range for absorption columns (0.5 to 0.7)[98,151] and may limit the unit efficiency, operation is still feasible.[151] It is also possible that the flue gas flow rate in the experimental studies was difficult to measure and, thus, potentially inaccurate, as reported by Kvamsdal and Rochelle

and by Faramarzi et al. in previous works.[124,145] Consequently, this may skew the flooding factor calculation, but, for consistency, we use the unadjusted, experimentally reported flow rates as was done in prior investigations of this absorption column. In all, this results in a thermochemical baseline scenario with a packing volume of 0.87 m^3 that is used to compare against the eCCC processes reported in this work.

4.2. Direct Capture Trends in Absorption Column Sizing

Given that direct eCCC is an emerging yet rapidly developing field, our objective is to use the absorption column model to help inform pathways towards achieving similar, if not smaller, unit sizes to those required for thermochemical processes. We use the packing volume as the metric of comparison, as this scales most directly with equipment costs.[123] To estimate the range of possible direct eCCC column sizes, we have identified several molecular properties and operating conditions that are still uncertain and if tuned to specific values, could lead to competitive column performance. Specifically, we vary $K_{1,direct}$, Da, [R_{tot}], Δx_a, and L/V. In addition to these five inputs, we separately investigate the impact of the capture fraction (α) on the final absorption column volume. While the thermochemical pilot-plant baseline (Run 32) was operated at α = 95%, it is likely that this value will ultimately be optimized to improve plant economics. We first perform a sensitivity analysis on each of the individual parameters to identify which of them have the greatest impact on the absorption column volume. To do this, we select the baseline values and ranges of variation for all parameters according to properties and operating conditions reported for model capture species (i.e., quinones) that have been studied as direct eCCC molecules.

Binding Coefficient ($K_{1,direct}$)

$K_{1,direct}$ has been studied extensively in the growing eCCC field. The range observed for various model quinones in several different solvents spans $\ln K_{1,direct}$ = 2.53 to $\ln K_{1,direct}$ = 45.82.[67] Across the compiled quinones from Zito et al., [67] the median value is $\ln K_{1,direct} = 13.12$, which we select as

our baseline and alter by ± 50% in the preliminary sensitivity study.

Damköhler Number (Da)

The values used for the dimensionless reaction rate constant, Da, were chosen based on the reaction rate constant data available in the peer-reviewed literature for similar solutions (i.e., quinones dissolved in PC-based electrolytes). Simpson and Durand reported the lowest second-order rate constant for CO_2 absorption via BQ in PC at 46 M^{-1} s^{-1} while the highest reported value was for CO_2 absorption by AQ in PC at 350 M^{-1} s^{-1}.[62] As discussed earlier, these rate constants apply to the reaction between CO_2 and the semiquinone, and thus may underestimate the reaction rate between the dianion and CO_2. Despite this, Xu et al. recently reported a strong, direct correlation between the binding coefficient ($K_{1,direct}$) and the rate of CO_2 uptake.[152] Given this and knowledge that BQ and AQ have high binding coefficients ($\ln K_{1,direct} = 38.91$ and $\ln K_{1,direct} = 27.17$, respectively), it is possible that these reported rate constants are relatively fast for reactions between semiquinones and CO_2. This large uncertainty in reaction rate constants led us to select a conservative range of Da values with a baseline set at Da = 100 (or $\log Da = 2$). This combined with a species diffusion coefficient of 4.2×10^{-10} m^2 s^{-1} results in a calculated rate constant of 40.1 M^{-1} s^{-1}, similar to the lowest rate constant reported by Simpson and Durand.[62] From this baseline, we alter the $\log Da$ by ± 50% (from $\log Da = 1$ to $\log Da = 3$), which results in rate constants ranging from 7.1 to 705.5 M^{-1} s^{-1}.

Capture Species Concentration ($[R_{tot}]$)

The values of $[R_{tot}]$ were selected based on a combination of solubility data from reported quinone species as well as targets established for other nonaqueous electrochemical systems such as RFBs.[153] While solubility data for quinones used in carbon capture applications are not widely available, Diederichsen et al. reported liquid quinones with concentrations > 1.1 M when mixed with low volatility glymes.[81] Additionally, researchers have reported quinone derivatives for use in both aqueous

and nonaqueous RFBs, in some cases, realizing solubilities of > 1 M in nonaqueous solvents like DMSO and ACN.[154–158] Consequently, we set the baseline [R_{tot}] to 1 M and vary it by ± 50%.

State-of-Charge Swing (Δx_a)

The Δx_a was selected based on knowledge from other electrochemical systems (i.e., lithium-ion batteries and RFBs), where operation from 0 to 100% state-of-charge ($\Delta x_a = 1$) is often associated with increased capacity fade rates due to extended time spent under extreme conditions.[159,160] We chose to set $\Delta x_a = 0.5$ (i.e., operate from 25 to 75% state-of-charge) as a baseline and vary it by ± 50%. This approach has also been taken in prior studies of direct eCCC.[50] By varying Δx_a by ± 50%, this sets the upper and lower bounds of the SoC swing to $\Delta x_a = 0.25$ and $\Delta x_a = 0.75$. When $\Delta x_a = 0.25$, the state-of-charge ranges from 37.5 to 62.5%, and when $\Delta x_a = 0.75$, the state-of-charge ranges from 12.5 to 87.5%. In each scenario, the state-of-charge oscillates about 50%.

Ratio of the Liquid to the Gas Mass Flow Rates (L/V)

To set the L/V baseline, we first determined that the MEA-based absorption system (Run 32) was run at an L/V value of 6.4; however, these processes often do not operate at large L/V values because of the increased energy requirements for the stripping unit.[111,161,162] Rather than bias our study by selecting values used in thermochemical systems, we were able to use acceptable ranges for F_{LV} reported across literature (**Section 3.1**) as well as system relevant flue gas and liquid stream densities to estimate that the column could operate from L/V = 0.16 to L/V = 94. While it is possible that higher flow rates may also lead to increased energetic requirements in eCCC, we chose to vary L/V over roughly half of this acceptable range such that the baseline was set at L/V = 50 and varied by ± 25.

Capture Fraction (α)

Finally, the capture fraction, α, was reported at 0.95 for the experimental study;[96,112] however, we vary this value between 0.91 and 0.99 capture to observe its impact on column size. While this variance is small compared to that of the other parameters, as mentioned earlier, optimal capture often occurs at

capture fractions > 0.90. Thus, operating within this confined range allows us to assess the probable operating conditions of such systems.[19,20]

Each of the above parameters, their baseline value, investigated ranges, and sources are listed in **Table 2**.

Table 2. Outline of the variations on relevant parameters in the sensitivity study on direct eCCC.

Metric	Baseline	Variation	Sources
$\ln K_{1,direct}$ (–)	13.12	± 6.56	Zito et al.[163]
$\log Da$ (–)	2	± 1	Mizen and Wrighton[90]; Simpson and Durand[62]; Xu et al.[152]
$[R_{tot}]$ (kmol m^{-3})	1	± 0.5	Diederichsen et al.[81]; Pahlevaninezhad et al.[154]
Δx_a (–)	0.5	± 0.25	Clarke et al.[50]; Wikner and Thiringer[159]; Roe et al.[160]
L/V (–)	50	± 25	Seader, Henley, and Roper[98]
α (–)	0.95	± 0.04	Dugas[112]; David et al.[19]; Rao et al.[20]

Given these ranges of interest, we first elect to vary each parameter individually, holding all others constant, to create a tornado plot of resulting absorber volumes (**Figure 4a**). While the column volume observed at the baseline condition (1.37 m^3) is larger than the thermochemical column volume (0.87 m^3), altering the input variables can reduce the required column size. We find that $\ln K_{1,direct}$ has the greatest impact on *increasing* the absorption column volume because, at sufficiently low binding coefficients (i.e., $\ln K_{1,direct} = 6.56$ for this analysis), the capture species can no longer bind enough CO_2 to achieve the baseline capture fraction ($\alpha = 0.95$), resulting in an infinitely-large column. Alternatively, the Da has a significant impact on both increasing and decreasing the column volume. This is because at higher rates of reaction relative to the rates of mass transfer in the film (i.e., higher Da values), the column can be much shorter due to lower residence time requirements. Furthermore, we observe that despite the small range studied, the operating capture fraction (α) can substantially change the absorber volume evincing the need for a full techno-economic assessment to determine optimal capture fraction, which is beyond the scope of this work. Lastly, Δx_a, L/V, and $[R_{tot}]$ all exert a lesser influence on the absorption column volume, but they remain viable tuning parameters for future studies.

In **Section 2.2**, we discussed model assumptions which were necessary to achieve desired capture fractions in the direct capture process. Specifically, we noted the possibility of assuming either chemical equilibrium ($K_{1,direct}$) or CO_2 phase equilibrium at the liquid outlet stream of the absorption column – two extremes that may arise depending on the CO_2 reaction and mass transfer rates. To validate these assumptions and quantify the effects that selecting one or the other would have on the final absorption column volume, we re-ran the sensitivity study from **Figure 4a** and compared the column heights that would result from assuming 1) chemical equilibrium or 2) phase equilibrium at the liquid outlet of the absorber. The results of this analysis, which appear in **Figure S7a**, reveal that the predicted absorption column heights deviate by ≤ 1.38% between the two sets of assumptions, indicating that the error is quite small. The largest errors are found in the Δx_a and Da sensitivity studies, specifically when these parameters are set to their lower bounds. We hypothesize that this phenomenon occurs at low values of Da because if we assume that the equilibrium constant, $K_{1,direct}$, applies, this implies that the reaction between the capture species and CO_2 occurs instantaneously, which inherently contradicts the conditions suggested by a low Da. Consequently, we maintain that, at high Da numbers ($Da \geq 10$, fast reaction), chemical equilibrium will apply, while at low Da numbers (slow reaction), phase equilibrium will apply.

Next, we individually investigate the trends in absorption column size associated with the full range of possible conditions for each of the parameters. Rather than limit the values studied to within a ~50% band of the baseline (or, in the case of the capture fraction, within a narrow band of expected values for optimal operation), we extend the study to the expected limits of each parameter. Thus, for the binding coefficient, we allow the lower limit of $\ln K_{1,direct}$ to approach 0 while the upper limit was set to approach 15, as a number of molecules (i.e., benzoquinone, naphthoquinone, anthraquinone, duroquinone, phenanthrenequinone, etc.) are capable of achieving $\ln K_{1,direct} \gg 15$.[67] We still investigate the effects of high binding coefficients on the absorption column volume despite their tendency for increased oxygen sensitivity that results from cathodically-shifted reduction peaks.[68] In **Figure 4b**, we initially observe a

marked reduction in column volume as the binding coefficient increases from the minimum viable value, but beyond intermediate values ($\ln K_{1,direct} > 9$), there are significantly diminishing reductions in column size. This suggests that while high binding coefficients may ensure that sufficient CO_2 is separated and lead to high faradaic efficiencies,[50] their benefit in reducing column size is limited. On the other extreme, however, if the binding coefficients are too small, the column size increases rapidly and approaches a regime where it is not possible to capture the desired quantity of CO_2. For example, if we consider a previously-studied direct eCCC molecule (i.e., tetrachloro-benzoquinone (TCBQ) dissolved in ACN), the binding coefficient is not large enough ($\ln K_{1,direct} = 5.76$) to capture 95% of the CO_2 in this selected system.[89] However, if other previously investigated molecules with higher binding coefficients such as tetrafluoro-1,4-benzoquinone ($\ln K_{1,direct} = 9.90$ in DMF), tetrabromo-1,4-benzoquinone ($\ln K_{1,direct} = 7.60$ in DMF), 5-hydroxy-naphthoquinone ($\ln K_{1,direct} = 7.60$ in ACN), or 2,6-dichloro-1,4-benzoquinone ($\ln K_{1,direct} = 13.82$ in ACN) were used in this system, it would be possible to successfully remove the desired amount of CO_2.[67]

An important observation in **Figure 4b** is also related to the trend in capture species concentration ($[R_{tot}]$) and its impact on the absorption column volume at low binding coefficient values. At low concentrations (0.46 M), the minimum achievable binding coefficient is ca. $\ln K_{1,direct} = 7.5$, but, at high concentrations (4 M), this minimum reduces to $\ln K_{1,direct} = 6.4$ – an order of magnitude reduction. The impact of solubility is thus exacerbated if the capture molecule has a relatively low binding constant. This can be exemplified by further contemplation of TCBQ, which exhibits a binding constant of $\ln K_{1,direct} = 6.84$ in 2 M ethanol and dimethylformamide (DMF),[80] slightly larger than its binding constant in ACN. At this binding constant, according to **Figure 4b**, the capture molecule must have a solubility of at least 1.2 M to successfully remove the desired amount of CO_2, reinforcing the importance of high solubilities. While the range of solubilities spans 0.46 M to 4 M in **Figure 4b**, we probed 10 concentration points spaced equally on a log scale between 0.25 and 4 M (0.25, 0.34, 0.46, 0.63, 0.86, 1.17, 1.59, 2.16, 2.94, and 4.00

M). Concentrations below 0.46 M are not shown on the figure because at these values, the system cannot capture enough CO_2 regardless of the binding coefficient. It is further evident that at the baseline conditions, varying $\ln K_{1,direct}$ and the species concentration cannot reduce the direct eCCC column size to below that of the comparable MEA capture column (0.87 m^3).

Unlike the binding coefficient, the column volume monotonically decreases with increasing Da, reinforcing the impact that reaction rates have on the column size (**Figure 4c**). Given constant fluid flow rates, the column height depends on how long it takes to capture the desired amount of CO_2. Increasing the Da (and consequently the rate of reaction between CO_2 and the sorbent species) can decrease the time scale for CO_2 absorption, lowering the required residence time and enabling a smaller column. Furthermore, we observe that when $Da > 300$ and the concentration of the capture species is at least 4 M, it is possible for the direct eCCC absorption column to be the same size or smaller than the baseline MEA column. While a 4 M capture species solution may be difficult to realize, our analysis indicates that at $Da \geq 10^3$, lower concentrations of at least 0.86 M would enable a competitive column, thereby reducing the solubility requirements. To contextualize these results against previously-studied rate constants, we estimate that Da numbers can range from Da = 8.5 for phenanthrenequinone in DMSO ($k_{1,f,direct}$ = 6.00 M^{-1} s^{-1}) to Da = 496.1 for anthraquinone in DMSO ($k_{1,f,direct}$ = 350 M^{-1} s^{-1}) (**Table S3**). If realized rate constants are at the upper end of these values, **Figure 4c** suggests that the absorption column for eCCC could become a drop-in replacement for current amine capture systems when capture species solubilities are above 1.17 M. Accordingly, as molecular discovery and development continues in this field, we emphasize the need to study the CO_2 uptake rates with both the semiquinone and the dianion in order to better quantify their rate constants.

Additional trends that result from varying α, Δx_a, and L/V parameter values are included in **Figure S8**. First, the capture fraction (**Figure S8a)** follows expected trends whereby increases in α lead to larger column sizes; however, we do not expect to operate at low capture fractions thus ultimately optimal capture

fractions must be determined from investigating the operating and capital cost trade-offs. We observe that both Δx_a and L/V exhibit similar diminishing returns with increasing magnitude (**Figures S8b** and**Error! Reference source not found. S8c**); however, we also note that when Δx_a is above 0.85, the lowest concentration studied (0.25 M) can capture sufficient quantities of CO_2. While this may enable the use of low solubility species, the selection of Δx_a will also require additional optimization in coordination with the electrochemical reactor performance and associated energy costs.

To this point, we have discussed the predicted absorption column sizes that would result from the conditions set in the model without regard for physical column design limitations. Textbooks recommend that the ratio of the height to the diameter should be between 1 and 30 and the height of the absorption column should not exceed 60 m to avoid wind load and foundation concerns.[164] That said, the Dangote distillation column in Nigeria has a height of 112 m,[165] suggesting that the design guidelines may be exceeded. The dashed, colored lines depicted in **Figure 4b** and **c** indicate operating regions that do not align with design guidance if a single column were to be used. Across most conditions studied, the direct capture process falls within the specification; however, at very low Da, the height-to-diameter ratios rise above the upper limit. The slower reaction rates relative to the rate of mass transport lead to increases in the absorption column height; however, according to the reported reaction uptake rate constants, the Da numbers would ideally be much larger (i.e., $Da \gg 1$), resulting in feasible sizes (**Figure 4c**, inset). Similar trends are observed in the other parameters studied for the direct capture process (**Figure S8**). We also note that the absorption columns considered here are for application at a pilot-scale plant, and thus their diameters and heights are more likely to meet the requirements due to smaller volumes of process gas to handle. As the process is scaled to larger systems (i.e., plant-scale applications), the diameter will likely expand to accommodate greater fluid flows, impacting the column height. In the future, studies of these column sizes should be performed for all proposed systems to assess manufacturing feasibility.

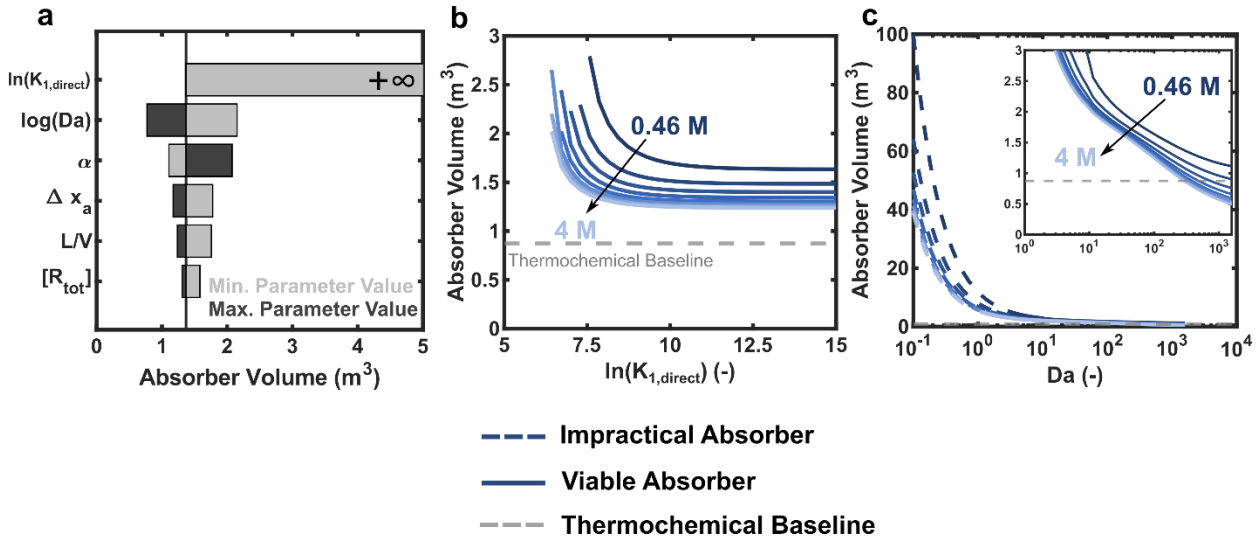

Figure 4. Impacts of material properties and operating conditions on the direct eCCC absorption column packing volume. (a) Tornado plot created from the sensitivity study on the parameters according to the conditions outlined in the text and **Table 2**. Light grey bars indicate the parameters are at their smallest value studied while the dark grey bars are at the largest studied value. (b) Impacts of $K_{1,direct}$ and (c) Da on the required absorber packed volume across a range of concentrations (0.25, 0.34, 0.46, 0.63, 0.86, 1.17, 1.59, 2.16, 2.94, and 4.00 M). Concentration increases are indicated by a color change from dark to light and emphasized by the labels in each plot. For each panel in (b) and (c), all other parameters are held constant at the baseline value while the single parameter is varied. The dashed blue lines represent absorption columns that are impractical to physically implement if a single column were desired. The dashed gray lines indicate the column size of the thermochemical baseline that is associated with a MEA-based thermochemical unit that can capture the same amount of CO_2 from an identical flue gas stream.

4.3. Indirect Capture Trends in Absorption Column Sizing

For the indirect capture process, we conducted the same sensitivity analysis as with the direct capture process; however, unlike the direct capture process, the reaction rates and equilibrium constants are fully defined in the indirect eCCC CO_2 uptake step. Consequently, pKa_1 and pKa_2 are the primary molecular properties that can be tuned for the redox-active mediator species (Q). While, to a certain extent, these pKa values can be independently tailored through molecular design, the second acid dissociation constant (Ka_2) must always be greater than or equal to the first acid dissociation constant (Ka_1) because it will always be more difficult to remove protons from a species with a higher electronegativity. Consequently, as a first pass in the sensitivity study, we assume that $pKa_1 = pKa_2$. Like the direct capture process, we chose quinones as model redox mediator compounds to establish baseline pKa values. According to a compilation of

quinone data reported by Huynh et al., the average values for pKa_1 and pKa_2 of solubilized quinones are 9.5 and 11.8, respectively.[166] Given these averages, we set $pKa_1 = pKa_2 = 11.8$ as a baseline value in the study and vary by ± 41% (± 4.8). This range was selected to maintain the pKa within reasonable bounds, given that 7.2 is the lowest pKa_1 value reported in the aforementioned publication.[166] For each of the other operating conditions varied ($[Q_{tot}]$, Δx_a L/V, and α), the sensitivity study was performed about the same baseline values and with the same deviations from the baseline as with the direct capture process. These input parameters are shown in **Table 3**.

Table 3. Outline of the variations on relevant parameters in the sensitivity study on indirect eCCC.

Metric	Baseline	Variation	Citation
pKa (–)	11.8	± 4.8	Huynh et al.[166]
$[Q_{tot}]$ (kmol m^{-3})	1	± 0.5	Yang et al.[157]; Zhang et al.[158]
Δx_a(–)	0.5	± 0.25	Clarke et al.[50]; Wikner and Thiringer[159]; Roe et al.[160]
L/V (–)	50	± 25	Seader, Henley, and Roper[98]
α (–)	0.95	± 0.04	Dugas[112]; David et al.[19]; Rao et al.[19,20]

To investigate the validity of assuming that either chemical ($K_{1,indirect}$) or phase equilibrium apply at the indirect absorption column outlet, we performed the same analysis as in the direct capture process to quantify the error between assumptions (**Figure S7b**). For the indirect capture process, we find that the error between the methods has a near negligible impact on the final absorption column volume. The largest error occurs when evaluating Δx_a, but this is only an error of 0.26%. While, in principle, we could apply chemical or phase equilibrium at the outlet of the absorption column, for the remainder of this work, we assume phase equilibrium applies given the slower CO_2 uptake reaction.

The tornado plot in **Figure 5a** highlights the impact that varying material properties and operating conditions has on the absorber volume in an indirect eCCC process. First, we note that the baseline absorber packing volume is larger than that for the direct capture process (5.01 m^3 vs. 1.37 m^3, respectively), which is likely due to the lower CO_2 fluxes entering the column caused by slower rates of reaction. At the baseline

conditions near the bottom of the column, the reaction rate with CO_2 is ~8.7×10^{-3} mol L^{-1} s^{-1} in the direct capture process while this value drops to ~1.5×10^{-4} mol L^{-1} s^{-1} in the indirect capture process. We find that varying each of the parameters in the indirect eCCC process results in a wide range of absorber volumes – a much larger range than the direct eCCC process (**Figure S9**). For the input parameters that were altered in *both* eCCC processes (i.e., α, Δx_a, L/V, and total redox-active species solubility), the most a single parameter affects the volume in direct eCCC is by 0.706 m^3 for α, while varying α in the indirect capture process increases the absorber volume by 2.6 m^3. Each of the other variables (Δx_a, L/V, and total redox-active species solubility) also lead to a larger volume change for the indirect column. We note that while the baseline conditions were selected using the best available knowledge, the stated observations and trends are strongly dependent on these baseline values for both processes. For instance, if the baseline value for $\log Da$ in the direct capture process were lowered from 2 to 1, the CO_2 uptake rate would be slower, necessitating a larger column size (2.15 m^3 as opposed to 1.37 m^3 from **Figure 4a**). This change in the baseline condition heightens the sensitivity of the column size to changes in the other input variables (**Figure S10**). For example, when we vary α at a constant $\log Da = 1$, the column volume could increase by as much as 1.15 m^3; however, when $\log Da = 2$, the volume range spans only 0.706 m^3. Given this observation, it is possible that changing the baseline conditions could alter our finding that the indirect process has a greater sensitivity to each variable.

Of the parameters varied, pKa has the greatest impact on column size; however, increasing its value cannot lead to conditions where the absorber volume is less than or equal to that reported for the baseline thermochemical system (**Figure 5b**). Despite this, at a given active species concentration, increasing both pKa_1 and pKa_2 to values ≥ 12 can significantly reduce the absorption column size, as predicted, and originally observed, in **Figure 5a**. At the elevated pKa values, we also see that concentration plays a significant role in enabling more competitive columns, as the volume drops from 2.83 to 1.02 m^3 (a 64% reduction) when the concentration increases from 0.25 to 4 M at pKa = 16. Since Δx_a also influences the amount of redox-active species available to alter the pH, we observe similar trends when increasing Δx_a,

as exhibited in **Figure 5a** and **Figure S11b**. We postulate three reasons why the concentration and state-of-charge swing have greater effects on the absorber size in the indirect capture process, as compared to the direct capture process. First, as we previously discussed, the magnitude of the absorber volume change is dependent on the selected baseline conditions. Second, the indirect involvement of the redox species on the binding and release of CO_2 in the pH-swing process can limit CO_2 capture efficiencies. For every capture species reduced in the direct eCCC process, we expect that 1 or 2 molecules of CO_2 (i.e., q) should be captured; however, this relationship in the indirect process is more ambiguous, as the reduction of the mediator species will result in a pH-swing that is dependent on the pKa values. Ultimately, the achievable pH then controls the rate of CO_2 uptake in the absorption column according to **Eq. 2.11a**, suggesting a nonlinear effect on column sizing. Third, and finally, the incremental impact of concentration on column size evolves as the pKa is increased. As the pKa values increase to the point that the absorber size plateaus, an operating regime where most of the protons in solution can bind with available reduced quinones is achieved. Once this is realized, the relative importance of the mediator species concentration on further improving the column size increases. This contrasts with the direct eCCC process, as the capture species always directly impact the rate of CO_2 uptake.

Further effects of α, Δx_a, and L/V ratio on the column size are presented in **Figure S11**. These follow similar trends to the direct capture process; however, a key difference is the ability for lower mediator species concentrations (i.e., 0.25 M) to capture sufficient CO_2 across the ranges studied. In the direct capture process, the maximum CO_2 capacity is set by the concentration of the capture species in solution, thus low concentrations may not feasibly capture enough CO_2 to achieve the desired capture fraction. However, in the indirect capture process, while low concentrations cannot achieve large pH swings and thus lead to larger columns, they can still successfully capture enough CO_2.

Unlike the direct capture process, the indirect capture process does not meet design guidelines (height-to-diameter ratio between 1 and 30 and height less than 60 m) across many of the conditions studied (**Figure**

5b) due to the slower reaction rates. This suggests that even if the increased capital costs caused by larger column sizes do not impede the implementation of an indirect process for a 4–stage PCC application, the absorber size requirements may demand that two or more columns are installed. Specifically, the inset of **Figure 5b** highlights that when $pKa_1 = pKa_2$ values fall below 12, a single absorber is no longer viable for the modeled pilot plant; however, as the column size approaches that of the thermochemical system, (i.e., as pKa values increase), conditions become increasingly favorable for practical design. Similar trends are observed in the other parameters studied (**Figure S11**).

To probe the effects that assuming $pKa_1 = pKa_2$ has on the column size, we chose to independently vary pKa_1 and pKa_2 over a range of relevant pKa values for quinone compounds (**Figure 5c**). The minimum values for pKa_1 and pKa_2 of solubilized quinones reported by Huynh et al. are 7.2 and 10, respectively, while the maximum reported value are 11.18 and 13, as evidenced by the gray triangles in **Figure 5c**.[166] While quinones are a good model chemistry, the reported dataset is only a subset of all possible quinone species that can be used in the pH-swing system. Additionally, there are other redox-active molecules capable of inducing the pH-swing mechanism such as alkoxides and phenoxides.[167] These two aforementioned points suggest that there will likely be pKa values that fall outside of the initial range reported by Huynh et al., therefore, we chose to extend the ranges to $pKa_1 = 6–14$ and $pKa_2 = 7–14$ while maintaining the constraints that $pKa_1 < pKa_2$ and all other input parameters are held at their baseline values (i.e., $[Q_{tot}] = 1$, $\Delta x_a = 0.5$, L/V =50, and $\alpha = 0.95$). **Figure 5c** displays the contour plot of required absorption column volumes that result from varying the pKa values within these ranges. It is evident that at these conditions, the absorber size is most impacted by pKa_2 across all pKa_1 values, indicating that a sufficiently high pH (and thus CO_2 uptake rate) can be achieved at the column inlet even if a single proton is taken up by Q (i.e., QH^- is favored in its equilibrium with Q^{2-}). If, however, the mediator species concentration is dropped to 0.25 M, we see that pKa_1 has a larger effect on the column size because there are less mediator species available to bind protons (**Figure S12**). Specifically, in this lower concentration scenario, both proton uptake reactions (i.e., **Eq. 14** and **Eq. 15**) are required to sufficiently swing the pH.

This is evinced by studying the pH of Stream 4 at the column inlet (**Figure S13**) as the pH associated with high (1 M) and low (0.25 M) mediator species concentrations is directly related to the absorber sizes reported in **Figure 5a** and **Figure S12**. As expected, the larger the pH, the smaller the unit. Additionally, when comparing the difference in pH at the same pKa values for the two concentrations, the pH is larger in the system with a higher concentration. This is attributed to the uptake of more protons across the system due to elevated concentrations of the mediator species, agreeing with our hypothesis.

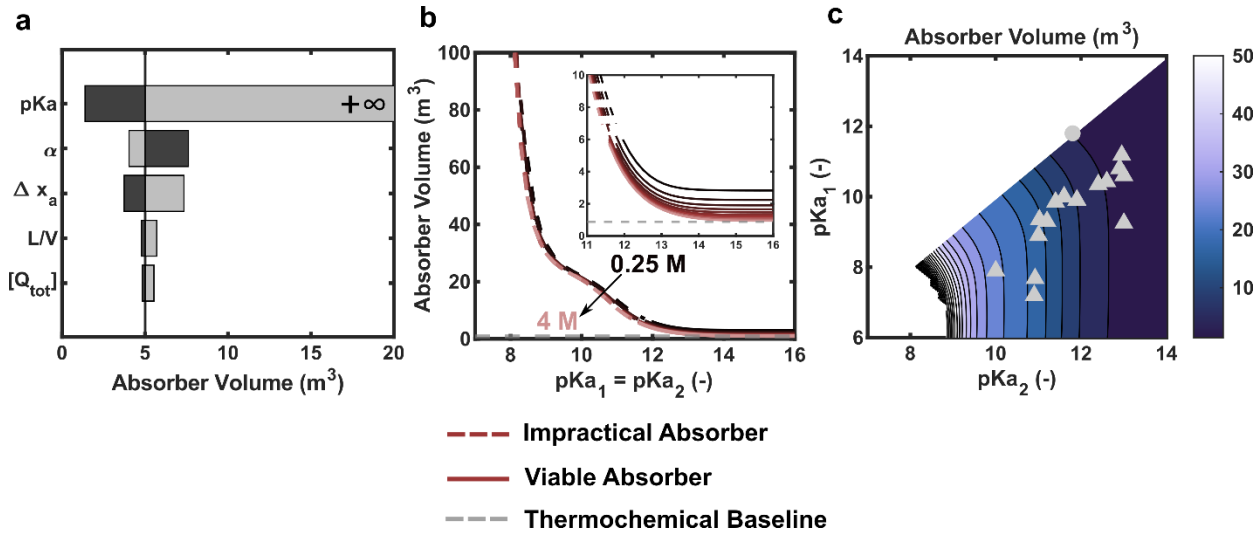

Figure 5. Impacts of material properties and operating conditions on the indirect eCCC absorption column packing volume. (a) Tornado plot created from the sensitivity study on the parameters according to the conditions outlined in the text and **Table 3**. Light grey bars indicate the parameters are at the smallest value studied while the dark grey bars are at the largest studied value. (b) Impacts of pKa on the required absorber packed volume across a range of concentrations (0.25, 0.34, 0.46, 0.63, 0.86, 1.17, 1.59, 2.16, 2.94, and 4.00 M). Concentration increases are indicated by a change in color from dark to light and emphasized by the labels in each plot. All other parameters are held constant at their baseline values while the pKa and concentration are varied. The dashed red lines represent absorption columns that are impractical to implement if a single column were desired. The dashed gray lines indicate the column size of the thermochemical baseline that is associated with a MEA-based unit that can capture the same amount of CO_2 from an identical flue gas stream. (c) Contour plot outlining the simultaneous impact that pKa_1 and pKa_2 have on the absorption column size. The gray triangles represent the pKa values associated with quinones as outlined in Huynh et al.[166] while the gray circle represents the baseline condition studied in all prior analyses ($pKa_1 = pKa_2 = 11.8$).

4.4. Consideration of Relevant Operating Conditions

As discussed, per the reported flow rates and absorption column diameters for the thermochemical baseline system, we determined that the pilot plant was experimentally operated at a flooding fraction of 0.269. However, flooding fractions for absorption columns often fall between 0.5 and 0.8,[98,123] suggesting that mass transport may not be optimized for the process studied. Accordingly, we relax the assumption that the column flooding fraction should equal that used in the thermochemical model by varying the flooding fraction from 0.05 to 0.8 (**Figure S14Error! Reference source not found.**). The eCCC column volumes that result decrease with increasing flooding fraction. While this does not enable direct comparisons with the experimentally studied thermochemical system, we can see that by increasing the fraction of flooding to relevant absorber ranges, the columns can be much smaller. This may ultimately allow a single column train to be used for more indirect capture conditions.

In addition to varying the flooding fraction, it is also likely that these capture platforms will be used in alternative industrial applications (i.e., other fossil fuel plants, cement facilities, steel mills, etc.) with varying CO_2 inlet concentrations. Specifically, as previously mentioned, flue gas streams can vary from 3 to 30% CO_2. If we allow the direct eCCC capture process to maintain the same operating conditions but simply vary the CO_2 inlet concentration, we observe that the column diameter increases from 0.56 m at 3% CO_2 to 0.65 m at 30% CO_2. On the other hand, as the CO_2 concentration increases, the driving force for mass transfer increases, causing the column height to decrease from 6.25 m to 3.69 m. Overall, these changes result in column volumes of 1.54 m^3 and 1.22 m^3 at 3 and 30% CO_2, respectively, exemplifying the benefits that higher concentration flue gas streams can have on required capital investments. Similar trends are observed in the indirect capture process.

4.5. Monte Carlo Investigation: Comparison to Absorber Sizes Reported in Literature

Comparisons between eCCC absorption columns and thermochemical absorption columns are necessary when determining their potential as drop-in replacements or for ultimately achieving similar, if

not lower, capital costs. The large capital costs associated with thermochemical capture systems suggest that reducing the absorption column size in eCCC would benefit the economics substantially. Unfortunately, given the current baseline values studied above, neither the direct (1.37 m^3) nor the indirect (5.01 m^3) eCCC processes can achieve an absorption column that is smaller than that of the MEA-based capture system (0.87 m^3). However, the baseline conditions represent a single data-point and the sensitivity studies were performed by changing a single input variable. Further insight can be derived from the column sizes that result from simultaneously varying all possible molecular properties and operating conditions for the direct and indirect eCCC processes.

To probe the uncertainty in the molecular properties of either the capture or mediator species and the system operating conditions that will be employed at scale, we performed a Monte Carlo analysis to measure the range of absorber packing volumes that result from altering each of the input parameters over a predicted distribution of values. For each of the input parameters, a random sample of 1000 values was taken from a normal distribution with a mean equal to the baseline values in **Table 2** and **Table 3** and a relative standard deviation of 0.2 for $\ln K_{1,direct}$, $\log Da$, $[R_{tot}]$, $[Q_{tot}]$, L/V, and Δx_a. For $pKa_1 = pKa_2 = pKa$, the distribution maintained a mean still equal to the pKa baseline set in **Table 3**, but a standard deviation of 0.1 was selected to avoid unreasonably low/high pKa values. For this analysis, we set the capture fraction at 0.95 to ensure the same CO_2 uptake as the thermochemical baseline. Sample distributions of $\log Da$ and pKa are presented in **Figure 6a** and **Figure 6d**, respectively, while all other distributions for the other input variables are included in **Figure S15** and **Figure S17**.

For the direct capture process, we observe that it is possible for the column to achieve a packing volume less than or equal to the thermochemical baseline values under several of the conditions studied (**Figure 6b**). We investigate this further by producing scatter plots of each variable input against the resulting absorption column size. These graphs facilitate the identification of correlations between input and output variables, helping to elucidate properties that are critical for achieving desired outcomes within a

multidimensional design space. In **Figure 6c**, we observe that the value of $\log Da$ has a strong negative correlation with the column size – stronger than any of the other input parameters (**Figure S16**). This finding corroborates the prior sensitivity studies and indicates that if $\log Da > 3$ (i.e., $Da > 10^3$), the direct eCCC process may achieve competitive column sizes that approach or surpass those required for thermochemical processes.

For the parameter ranges selected, there are no input combinations that result in an indirect capture process column size that is less than or equal to the thermochemical baseline (**Figure 6e**). The scatter plots suggest that altering the pKa has the greatest impact on unit size (**Figure 6f** and **Figure S18**); however, diminishing returns mean the thermochemical target cannot be met. Again, these results agree with the earlier sensitivity analyses.

The strong correlations between the absorption column heights and the Da and pKa for the direct and indirect capture processes, respectively, not only agree with earlier findings in this work but also align with our expectations for efficient absorption column operation. Specifically, for both processes, varying these inputs is the most direct way to increase the reaction rate with CO_2 (Da is a proxy for the reaction rate constant while pKa can alter the reaction conditions through the pH regulation). Given the deviation from the mean at each Da and pKa value in the Monte Carlo analyses (**Figure 6c** and **Figure 6f**), once a molecule has been identified and its reaction rate constants quantified, further optimization within the studied parameters and operating conditions (i.e., $[R_{tot}]$, $[Q_{tot}]$, L/V, Δx_a, and $\ln K_{1,direct}$) may, to a lesser degree, impact both the absorption column size and the energetic requirements of the system.

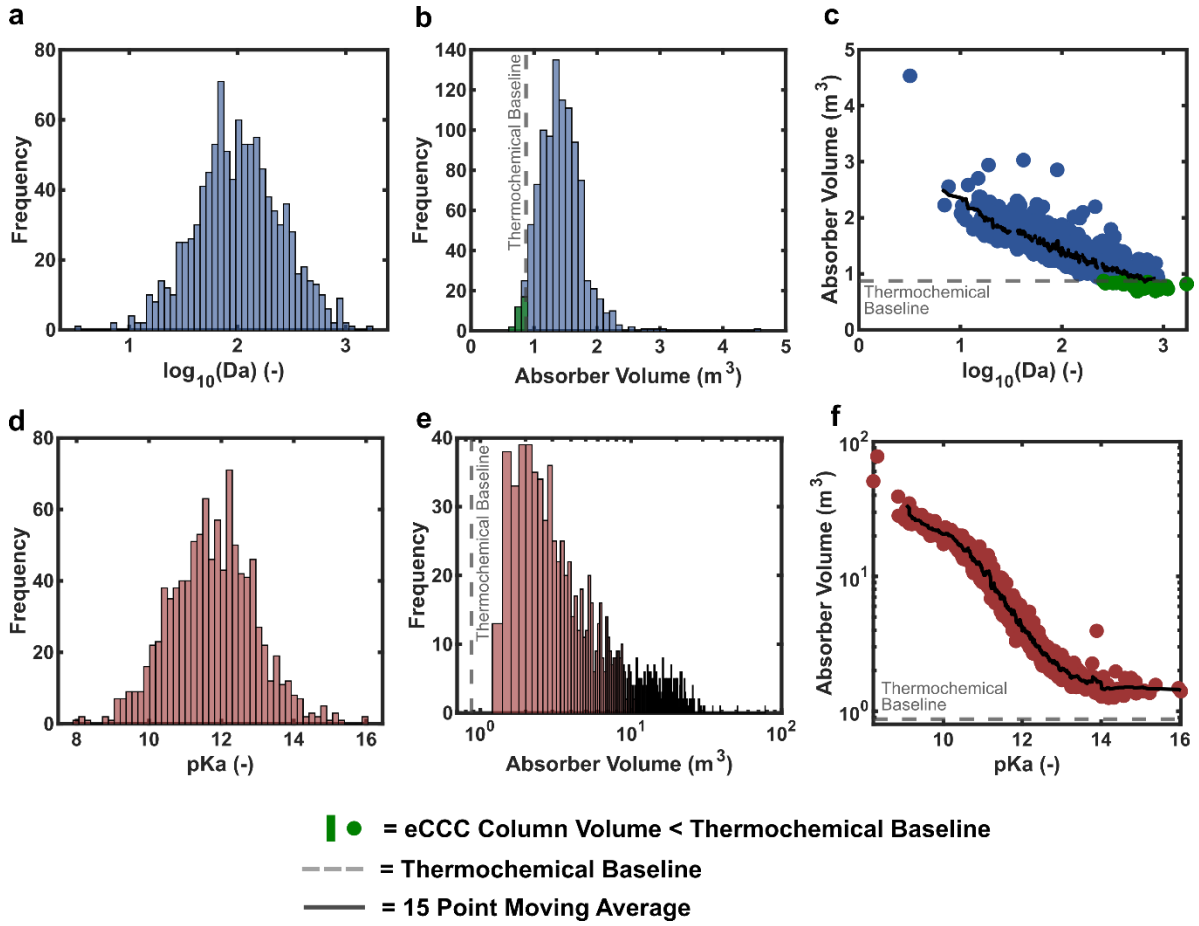

Figure 6. Monte Carlo simulation results for the direct capture process based on (a) normal distributions of input variables ($\log Da$ is displayed here; $\ln K_{1,direct}$, $[R_{tot}]$, L/V, and Δx_a are presented in **Figure S15**). (b) The resulting distribution of column sizes that result from 1000 random combinations of the direct eCCC input variables. (c) Scatter plot revealing a correlation between $\log Da$ and the resulting absorber volumes in each of the simulation runs ($\log Da$ is displayed here; $\ln K_{1,direct}$, $[R_{tot}]$, L/V, and Δx_a are presented in **Figure S16**). Monte Carlo simulation results for the indirect capture process based on (d) normal distributions of input variables (pKa is displayed here; $[Q_{tot}]$, L/V, and Δx_a are presented in **Figure S17**). (e) The resulting distribution of column sizes on a log scale that result from 1000 random combinations of the indirect eCCC input variables. (f) Scatter plot revealing a correlation between pKa and the resulting absorber volumes in each of the simulation runs (pKa is displayed here; $[Q_{tot}]$, L/V, and Δx_a are presented in **Figure S18**). Green data points reveal regions of the eCCC processes that result in volumes that are equal to or less than the thermochemical baselines (gray dashed line). The solid black lines in (c) and (f) represent a 15-point moving average.

5. Conclusions

In this work, we developed an absorption column model to predict the required absorber height and diameter for thermochemical, direct electrochemical, and indirect electrochemical CO_2 separation processes. This model is designed to generally apply to any soluble capture or mediator species that may be used in eCCC systems. We investigate the effects of various input parameters, including binding coefficients, state-of-charge swings, solubility, flow rates, reaction rate constants, and pKa values, on the absorber volume and explore how these variables can be adjusted to meet specific column design targets in eCCC processes. Specifically, we note that the parameters most aligned with the reaction uptake rate of CO_2 (Da and pKa) have the greatest effect on absorption column volumes in both direct and indirect eCCC. In order to minimize the column size, these values should be maximized. We also observe that the direct capture process could be used in a retrofit application, as it can achieve column sizes that are similar to those associated with the comparable thermochemical system. However, if indirect eCCC systems are ultimately deployed, such drop-in-replacement options may not be feasible given the larger column requirements.

While the work presented herein can be used to compare absorption column sizes and, consequently, differences in system capital costs, a full comparison between state-of-the-art alkanolamine capture technologies and proposed eCCC platforms will require techno-economic analyses to calculate both capital and operating costs associated with all process units within 4-stage eCCC and thermochemical processes. While we outline possible pathways towards column sizes that are competitive with those of thermochemical systems, the capital costs associated with these units are only one component of the total system costs. Future studies will need to incorporate the absorption column into cost analyses where trade-offs with operating costs associated with the energy requirements are expected to impact economic feasibility. In these endeavors, relationships between cell / stack operating current densities and voltages can be coupled with the model developed here to better assess performance and costs across different eCCC platforms. The potential for significant energetic benefits in eCCC could allow greater flexibility in the ultimate absorption column size for 4-stage eCCC systems.

6. Author Information

Corresponding Author

Fikile R. Brushett - *Department of Chemical Engineering, Massachusetts Institute of Technology, Cambridge, Massachusetts 02139, United States*; Email: brushett@ mit.edu

Author

Katelyn M. Ripley - *Department of Chemical Engineering, Massachusetts Institute of Technology, Cambridge, Massachusetts 02139, United States*

7. Author Contributions

K.M.R.: Conceptualization, methodology, validation, formal analysis, investigation, data collection, data analysis, writing (original draft), writing (review and editing), and visualization. F.R.B.: Conceptualization, resources, writing (original draft), writing (review and editing), supervision, and funding acquisition.

8. Notes

The authors declare no competing financial interest.

9. Supporting Information

The supporting information includes derivations of the material balances, absorption column plug-flow model, and two-film model used in the main text. We also include the specific correlations and metrics used in the thermochemical, direct eCCC, and indirect eCCC systems. Additional model outputs from the validation, sensitivity studies, and Monte Carlo simulations are also included.

10. Acknowledgements

This work was supported by the Alfred P. Sloan Foundation and by the Exxon Mobil Corporation. K.M.R gratefully acknowledges the support of the Department of Defense National Defense Science and

Engineering Graduate (NDSEG) Fellowship. We thank our collaborators Prof. Jenny Yang and Prof. Anastassia Alexandrova from UC Irvine and UCLA, respectively, and their group members for their feedback during this project. We also thank Lauren Clarke and Isabella Caruso of the Brushett Group for their helpful recommendations and discussions. Finally, we thank Dr. Steve Reece of Lockheed Martin Advanced Energy Storage for his helpful insights on the technoeconomic considerations of the systems considered here.

11. Glossary of Terms

Nomenclature

a_w	effective interfacial area of packing per unit volume ($m^2\ m^{-3}$)
A	column cross-sectional area (m^2)
Bo	Bodenstein number (–)
C_0	standard concentration (1 mol L^{-1})
d_p	packing material diameter (m)
D_{abs}	absorber diameter (m)
$\mathcal{D}_{ax}$	axial dispersion coefficient ($m^2\ s^{-1}$)
$\mathcal{D}_i$	diffusion coefficient if species *i* in solution ($m^2\ s^{-1}$)
Da	Damköhler number (–)
DIC	dissolved inorganic carbon (mol L^{-1})
f	fraction of flooding in the absorption column (–)
F_C	empirical factor for determining correlations between column pressure drop and F_{LV} to determine the column diameter (–)
F_{LV}	liquid-gas kinetic energy factor (–)
h_L	liquid hold-up (liquid volume per unit volume packing) in the column ($m^3_{liquid}\ m^{-3}_{packing}$)
H_{CO_2}	Henry's law constant for CO_2 (kmol m^{-3} bar^{-1})
$[\,i\,]$	concentration of species *i* in the solution (mol L^{-1})
k_G	gas film mass transfer coefficient (kmol $m^{-2}\ s^{-1}$ bar^{-1})
k_L	liquid film mass transfer coefficient ($m\ s^{-1}$)
$k_{1,f}$	forward second order rate constant for the CO_2 absorption (m^3 $kmol^{-1}\ s^{-1}$)
$k_{2,f,indirect}$	forward second order rate constant for the reaction between H^+ and CO_3^{2-} (m^3 $kmol^{-1}\ s^{-1}$)
$k_{w,f}$	forward second order rate constant for the reaction between H^+ and OH^- (m^3 $kmol^{-1}\ s^{-1}$)
$k_{Q,1,f}$	forward second order rate constant for the reaction between H^+ and QH^- (m^3 $kmol^{-1}\ s^{-1}$)
$k_{Q,2,f}$	forward second order rate constant for the reaction between H^+ and Q^{2-} (m^3 $kmol^{-1}\ s^{-1}$)
$K_{1,direct}$	binding coefficient of R^{n-} relative to dissolved CO_2 (–)
$K_{2,direct}$	binding coefficient of R relative to dissolved CO_2 (–)

$K_{1,indirect}$	equilibrium constant between CO_2 and HCO_3^- in aqueous conditions (–)
$K_{2,indirect}$	equilibrium constant between HCO_3^- and CO_3^{2-} in aqueous conditions (–)
K_w	water dissociation constant (–)
$K_{a,1}$	first acid dissociation constant for the mediator species (–)
$K_{a,2}$	second acid dissociation constant for the mediator species (–)
L	liquid mass flow rate (kg s^{-1})
L/V	liquid to gas mass flow rate ratio (–)
M	molecular weight (g mol^{-1})
n	moles of electrons transferred per mole of redox active species (mol e^- mol^{-1})
N_{CO_2}	flux of CO_2 across an interface in the thin-film (kmol m^{-2} h^{-1})
P_i	partial pressure of gaseous species *i* (bar)
P_0	total gas pressure (bar)
q	moles of CO_2 captured per mole of capture species in the direct capture process
$\dot{Q}$	volumetric flow rate (m^3 h^{-1})
$\mathbf{Q}$	generic mediator species used in the indirect capture process
$[\mathbf{Q}_{tot}]$	mediator species total concentration in the indirect capture process (mol L^{-1})
r_i	rate of consumption of species *i* (kmol m^{-3} h^{-1})
r_1	rate of reaction between CO_2 and the absorbent species (R^{n-} for the direct process, OH^- in the indirect process, and MEA in the thermochemical process) (kmol m^{-3} h^{-1} or kmol m^{-3} s^{-1})
$r_{2,direct}$	rate of CO_2 desorption from species R in the direct process (kmol m^{-3} s^{-1})
$r_{2,indirect}$	rate of reaction for reaction between H^+ and HCO_3^{2-} (kmol m^{-3} s^{-1})
r_w	rate of reaction for the reaction between H^+ and OH^- (kmol m^{-3} s^{-1})
$r_{Q,1}$	rate of reaction for the reaction between H^+ and QH^- (kmol m^{-3} s^{-1})
$r_{Q,2}$	rate of reaction for the reaction between H^+ and Q^{2-} (kmol m^{-3} s^{-1})
$\mathbf{R}$	generic capture species used in the direct capture process
$[\mathbf{R}_{tot}]$	capture species total concentration in the direct capture process (mol L^{-1})
$\mathbf{TA}$	total alkalinity (mol L^{-1})
u	fluid velocity (m s^{-1} or ft s^{-1})
V	gas mass flow rate (kg s^{-1})
$\bar{V}$	gas molar flow rate (kmol h^{-1})
x_a	state-of-charge of the solution (–)
Δx_a	state-of-charge swing of the redox-active species in solution (–)
Y	distance from the interface in the liquid-phase reaction boundary layer (m)
y_i	mole fraction of species *i* in the gas phase (–)
$\bar{y}_i$	average mole fraction of species *i* in the gas phase across the length of the column (–)
z	location along the height of the absorption column (m)

Greek symbols

α	CO_2 capture fraction (–)
δ	liquid boundary layer thickness (m)

$\boldsymbol{\mu}$	viscosity (Pa-s)
$\boldsymbol{\rho}$	density (kg m^{-3})
$\boldsymbol{\sigma}$	surface tension (N/m)
Subscripts	
b	bulk electrolyte property
direct	property of the direct capture process
flood	condition at flooding
G	gas-phase property
i	chemical species reference (i.e., *i* can represent CO_2, R, H_2O, MEA, etc.)
indirect	property of the indirect capture process
I	interfacial property
lit	reported literature values
L	liquid-phase solution property
m	stream reference number (can be 1-7)
MEA	property of the monoethanolamine (MEA) capture process
packing	property of the packing material
pred	values predicted by the model developed in this work

References

(1) Mullen, J.; Viscusi, G.; Chen, O.; Tapia, V. G.; Rogé, A.; Alvarez, C. F.; Hugues, P.; Kueppers, M.; Vautrin, A.; Arsalane, Y.; Bahar, H.; Chen, Y.; Collina, L.; Criswell, T.; Dubreuil, J.-B.; Healy, C.; Han, Y.; Jorquera, J.; Martin, A. R.; McGlade, C.; Molnar, G.; Bredariol, T. de O.; Sanchez, D. P.; Petropoulos, A.; Rosa, L. F.; Simon, R.; Spencer, T.; Wanner, B.; dos Santos, M. Despite Promising Growth in Renewables, Power Sector Emissions Had the Largest Sectoral Growth. In *CO2 Emissions in 2022*; IEA: Paris, 2023; p 9.

(2) Abdelilah, Y.; Bahar, A. A. B. H.; Bojek, P.; Briens, F.; Criswell, T.; Moorhouse, J.; Martinez, L. M.; Veerakumar, K. Chapter 1. Electricity. In *Renewables, 2023: Analysis and forecast to 2028*; IEA: Paris, 2024; p 14.

(3) U.S. Energy Information Administration. 1. The Electricity Mix in the United States Shifts from Fossil Fuels to Renewables. In *Annual Energy Outlook 2023*; EIA, 2023; pp 9–13.

(4) Pales, A. F.; Levi, P.; Remme, U.; Teter, J.; Abergel, T.; Bains, P.; Menendez, J. M. B.; Delmastro, C.; Gorner, M.; Gouy, A.; Malischek, R.; Mandova, H.; Morgan, T.; Paoli, L.; Tattini, J.; Vass, T.; Bibra, E.; Bunsen, T.; Connelly, E.; Fukui, H.; Hasegawa, T.; Leduc, P.; Pavan, F.; Wachche, S.; Widell, P.-A.; Abettan, C.; Hilton, C.; Koczka, R.; Louis, D.; IEA. Chapter 1: A New Era for CCUS. In *Energy Technology Perspectives 2020 - Special Report on Carbon Capture Utilisation and Storage*; IEA, 2020; pp 21–22. https://doi.org/10.1787/208b66f4-en.

(5) IPCC, 2023: Summary for Policymakers. In *Climate Change 2023: Synthesis Report. Contribution of Working Groups I, II and III to the Sixth Assessment Report of the Intergovernmental Panel on Climate Change*; Core Writing Team, Lee, H., Romero, J., Eds.; IPCC: Geneva, Switzerland, 2023; pp 1–34. https://doi.org/10.59327/IPCC/AR6-9789291691647.001.

(6) Habert, G.; Miller, S. A.; John, V. M.; Provis, J. L.; Favier, A.; Horvath, A.; Scrivener, K. L. Environmental Impacts and Decarbonization Strategies in the Cement and Concrete Industries. *Nat Rev Earth Environ* **2020**, *1* (11), 559–573. https://doi.org/10.1038/s43017-020-0093-3.

(7) Senate of the United States. *Inflation Reduction Act of 2022*; 2022; pp 1–725.

(8) Wang, M.; Lawal, A.; Stephenson, P.; Sidders, J.; Ramshaw, C. Post-Combustion CO2 Capture with Chemical Absorption: A State-of-the-Art Review. *Chemical Engineering Research and Design* **2011**, *89* (9), 1609–1624. https://doi.org/10.1016/j.cherd.2010.11.005.

(9) Hedin, N.; Andersson, L.; Bergström, L.; Yan, J. Adsorbents for the Post-Combustion Capture of CO2 Using Rapid Temperature Swing or Vacuum Swing Adsorption. *Appl Energy* **2013**, *104*, 418–433. https://doi.org/10.1016/j.apenergy.2012.11.034.

(10) Riboldi, L.; Bolland, O. Overview on Pressure Swing Adsorption (PSA) as CO2 Capture Technology: State-of-the-Art, Limits and Potentials. *Energy Procedia* **2017**, *114* (1876), 2390–2400. https://doi.org/10.1016/j.egypro.2017.03.1385.

(11) Falk-Pedersen, O.; Grønvold, M. S.; Nøkleby, P.; Bjerve, F.; Svendsen, H. F. CO2 Capture with Membrane Contactors. *Int J Green Energy* **2005**, *2*, 157–165. https://doi.org/10.1081/GE-200058965.

(12) Song, C.; Liu, Q.; Deng, S.; Li, H.; Kitamura, Y. Cryogenic-Based CO2 Capture Technologies: State-of-the-Art Developments and Current Challenges. *Renewable and Sustainable Energy Reviews* **2019**, *101* (November 2018), 265–278. https://doi.org/10.1016/j.rser.2018.11.018.

(13) Wang, X.; Song, C. Carbon Capture From Flue Gas and the Atmosphere: A Perspective. *Front Energy Res* **2020**, *8*, 560849. https://doi.org/10.3389/fenrg.2020.560849.

(14) Kanniche, M.; Gros-Bonnivard, R.; Jaud, P.; Valle-Marcos, J.; Amann, J. M.; Bouallou, C. Pre-Combustion, Post-Combustion and Oxy-Combustion in Thermal Power Plant for CO2 Capture. *Appl Therm Eng* **2010**, *30* (1), 53–62. https://doi.org/10.1016/j.applthermaleng.2009.05.005.

(15) Wang, Y.; Zhao, L.; Otto, A.; Robinius, M.; Stolten, D. A Review of Post-Combustion CO2 Capture Technologies from Coal-Fired Power Plants. *Energy Procedia* **2017**, *114* (November 2016), 650–665. https://doi.org/10.1016/j.egypro.2017.03.1209.

(16) Raganati, F.; Miccio, F.; Ammendola, P. Adsorption of Carbon Dioxide for Post-Combustion Capture: A Review. *Energy and Fuels* **2021**, *35* (16), 12845–12868. https://doi.org/10.1021/acs.energyfuels.1c01618.

(17) Halliday, C.; Hatton, T. A. Sorbents for the Capture of CO2 and Other Acid Gases: A Review. *Ind Eng Chem Res* **2021**, *60* (26), 9313–9346. https://doi.org/10.1021/acs.iecr.1c00597.

(18) Aaron, D.; Tsouris, C. Separation of CO2 from Flue Gas: A Review. *Sep Sci Technol* **2005**, *40* (1–3), 321–348. https://doi.org/10.1081/SS-200042244.

(19) David, J.; Herzog, H. The Cost of Carbon Capture. In *Fifth International Conference on Greenhouse Gas Control Technologies*; Cairns, Australia, 2000.

(20) Rao, A. B.; Rubin, E. S. Identifying Cost-Effective CO2 Control Levels for Amine-Based CO2 Capture Systems. *Ind Eng Chem Res* **2006**, *45* (8), 2421–2429. https://doi.org/10.1021/ie050603p.

(21) Luis, P. Use of Monoethanolamine (MEA) for CO2 Capture in a Global Scenario: Consequences and Alternatives. *Desalination* **2016**, *380*, 93–99. https://doi.org/10.1016/j.desal.2015.08.004.

(22) Freguia, S.; Rochelle, G. T. Modeling of CO2 Capture by Aqueous Monoethanolamine. *AIChE Journal* **2003**, *49* (7), 1676–1686. https://doi.org/10.1002/aic.690490708.

(23) Abu-Zahra, M. R. M.; Schneiders, L. H. J.; Niederer, J. P. M.; Feron, P. H. M.; Versteeg, G. F. CO2 Capture from Power Plants: Part I. A Parametric Study of the Technical Performance Based on Monoethanolamine. *International Journal of Greenhouse Gas Control* **2007**, *1* (1), 37–46.

(24) Lv, B.; Guo, B.; Zhou, Z.; Jing, G. Mechanisms of CO2 Capture into Monoethanolamine Solution with Different CO2 Loading during the Absorption/Desorption Processes. *Environ Sci Technol* **2015**, *49* (17), 10728–10735. https://doi.org/10.1021/acs.est.5b02356.

(25) Zhang, Y.; Chen, H.; Chen, C. C.; Plaza, J. M.; Dugas, R.; Rochelle, G. T. Rate-Based Process Modeling Study of CO2 Capture with Aqueous Monoethanolamine Solution. *Ind Eng Chem Res* **2009**, *48* (20), 9233–9246. https://doi.org/10.1021/ie900068k.

(26) Littel, R. J.; Versteeg, G. F.; Van Swaaij, W. P. M. Kinetics of CO2 with Primary and Secondary Amines in Aqueous Solutions-II. Influence of Temperature on Zwitterion Formation and Deprotonation Rates. *Chem Eng Sci* **1992**, *47* (8), 2037–2045. https://doi.org/10.1016/0009-2509(92)80320-C.

(27) Rinker, E. B.; Ashour, S. S.; Sandall, O. C. Absorption of Carbon Dioxide into Aqueous Blends of 2-Amino-2-Methyl-1-Propanol and Monoethanolamine. *Chem Eng Sci* **2000**, *39*, 4346–4356. https://doi.org/10.1016/j.ces.2006.04.002.

(28) Chowdhury, F. A.; Yamada, H.; Higashii, T.; Goto, K.; Onoda, M. CO2 Capture by Tertiary Amine Absorbents: A Performance Comparison Study. *Ind Eng Chem Res* **2013**, *52* (24), 8323–8331. https://doi.org/10.1021/ie400825u.

(29) Veawab, A.; Tontiwachwuthikul, P.; Bhole, S. D. Studies of Corrosion and Corrosion Control in a CO2-2-Amino-2-Methyl-1-Propanol (AMP) Environment. *Ind Eng Chem Res* **1997**, *36* (1), 264–269. https://doi.org/10.1021/ie9504563.

(30) Gouedard, C.; Picq, D.; Launay, F.; Carrette, P. L. Amine Degradation in CO2 Capture. I. A Review. *International Journal of Greenhouse Gas Control*. Elsevier September 1, 2012, pp 244–270. https://doi.org/10.1016/j.ijggc.2012.06.015.

(31) Chapel, D. G.; Mariz, C. L.; Ernest, J. Recovery of CO2 from Flue Gases: Commercial Trends. In *Canadian Society of Chemical Engineers Annual Meeting*; Saskatoon, Saskatchewan, Canada, 1999; p 17.

(32) Freeman, S. A.; Dugas, R.; Van Wagener, D. H.; Nguyen, T.; Rochelle, G. T. Carbon Dioxide Capture with Concentrated, Aqueous Piperazine. *International Journal of Greenhouse Gas Control* **2010**, *4* (2), 119–124. https://doi.org/10.1016/j.ijggc.2009.10.008.

(33) Alawode, A. O. Oxidative Degradation of Piperazine in the Absorption of Carbon Dioxide, The University of Texas at Austin, 2005.

(34) Oexmann, J.; Kather, A. Post-Combustion CO2 Capture in Coal-Fired Power Plants: Comparison of Integrated Chemical Absorption Processes with Piperazine Promoted Potassium Carbonate and MEA. *Energy Procedia* **2009**, *1* (1), 799–806. https://doi.org/10.1016/j.egypro.2009.01.106.

(35) Li, K.; Leigh, W.; Feron, P.; Yu, H.; Tade, M. Systematic Study of Aqueous Monoethanolamine (MEA)-Based CO2 Capture Process: Techno-Economic Assessment of the MEA Process and Its Improvements. *Appl Energy* **2016**, *165*, 648–659. https://doi.org/10.1016/j.apenergy.2015.12.109.

(36) Barzagli, F.; Mani, F.; Peruzzini, M. A Comparative Study of the CO2 Absorption in Some Solvent-Free Alkanolamines and in Aqueous Monoethanolamine (MEA). *Environ Sci Technol* **2016**, *50* (13), 7239–7246. https://doi.org/10.1021/acs.est.6b00150.

(37) Lawal, A.; Wang, M.; Stephenson, P.; Obi, O. Demonstrating Full-Scale Post-Combustion CO 2 Capture for Coal-Fired Power Plants through Dynamic Modelling and Simulation. *Fuel* **2012**, *101*, 115–128. https://doi.org/10.1016/j.fuel.2010.10.056.

(38) Li, K.; Cousins, A.; Yu, H.; Feron, P.; Tade, M.; Luo, W.; Chen, J. Systematic Study of Aqueous Monoethanolamine-Based CO2 Capture Process: Model Development and Process Improvement. *Energy Sci Eng* **2016**, *4* (1), 23–39. https://doi.org/10.1002/ese3.101.

(39) Maham, Y.; Teng, T. T.; Hepler, L. G.; Mather, A. E. Volumetric Properties of Aqueous Solutions of Monoethanolamine, Mono- and Dimethylethanolamines at Temperatures from 5 to 80 °C I. *Thermochim Acta* **2002**, *386* (2), 111–118. https://doi.org/10.1016/S0040-6031(01)00812-7.

(40) Bui, M.; Adjiman, C. S.; Bardow, A.; Anthony, E. J.; Boston, A.; Brown, S.; Fennell, P. S.; Fuss, S.; Galindo, A.; Hackett, L. A.; Hallett, J. P.; Herzog, H. J.; Jackson, G.; Kemper, J.; Krevor, S.; Maitland, G. C.; Matuszewski, M.; Metcalfe, I. S.; Petit, C.; Puxty, G.; Reimer, J.; Reiner, D. M.; Rubin, E. S.; Scott, S. A.; Shah, N.; Smit, B.; Trusler, J. P. M.; Webley, P.; Wilcox, J.; Mac Dowell, N. Carbon Capture and Storage (CCS): The Way Forward. *Energy Environ Sci* **2018**, *11* (5), 1062–1176. https://doi.org/10.1039/c7ee02342a.

(41) Strazisar, B. R.; Anderson, R. R.; White, C. M. Degradation Pathways for Monoethanolamine in a CO2 Capture Facility. *Energy and Fuels* **2003**, *17* (4), 1034–1039. https://doi.org/10.1021/ef020272i.

(42) House, K. Z.; Harvey, C. F.; Aziz, M. J.; Schrag, D. P. The Energy Penalty of Post-Combustion CO2 Capture & Storage and Its Implications for Retrofitting the U.S. Installed Base. *Energy Environ Sci* **2009**, *2* (2), 193–205. https://doi.org/10.1039/b811608c.

(43) House, K. Z.; Baclig, A. C.; Ranjan, M.; Van Nierop, E. A.; Wilcox, J.; Herzog, H. J. Economic and Energetic Analysis of Capturing CO2 from Ambient Air. *Proc Natl Acad Sci U S A* **2011**, *108* (51), 20428–20433. https://doi.org/10.1073/PNAS.1012253108/SUPPL_FILE/APPENDIX.PDF.

(44) Zhao, R.; Deng, S.; Liu, Y.; Zhao, Q.; He, J.; Zhao, L. Carbon Pump: Fundamental Theory and Applications. *Energy* **2017**, *119*, 1131–1143. https://doi.org/10.1016/j.energy.2016.11.076.

(45) Page, S. C.; Williamson, A. G.; Mason, I. G. Carbon Capture and Storage: Fundamental Thermodynamics and Current Technology. *Energy Policy* **2009**, *37* (9), 3314–3324. https://doi.org/10.1016/j.enpol.2008.10.028.

(46) Danaci, D.; Bui, M.; Petit, C.; MacDowell, N. En Route to Zero Emissions for Power and Industry with Amine-Based Post-Combustion Capture. *Environ Sci Technol* **2021**, *55* (15), 10619–10632. https://doi.org/10.1021/acs.est.0c07261.

(47) Huang, B.; Xu, S.; Gao, S.; Liu, L.; Tao, J.; Niu, H.; Cai, M.; Cheng, J. Industrial Test and Techno-Economic Analysis of CO2 Capture in Huaneng Beijing Coal-Fired Power Station. *Appl Energy* **2010**, *87* (11), 3347–3354. https://doi.org/10.1016/j.apenergy.2010.03.007.

(48) Sharifian, R.; Wagterveld, M.; Digdaya, I. A.; Xiang, C.; Vermaas, D. A. Electrochemical Carbon Dioxide Capture to Close the Carbon Cycle. *Energy Environ Sci* **2021**, *14*, 781–814. https://doi.org/10.1039/d0ee03382k.

(49) Shaw, R. A.; Hatton, T. A. Electrochemical CO2 Capture Thermodynamics. *International Journal of Greenhouse Gas Control* **2020**, *95*, 102878.

(50) Clarke, L. E.; Leonard, M. E.; Hatton, T. A.; Brushett, F. R. Thermodynamic Modeling of CO2 Separation Systems with Soluble, Redox-Active Capture Species. *Ind Eng Chem Res* **2022**, *61* (29), 10531–10546. https://doi.org/10.1021/acs.iecr.1c04185.

(51) Gurkan, B.; Su, X.; Klemm, A.; Kim, Y.; Mallikarjun Sharada, S.; Rodriguez-Katakura, A.; Kron, K. J. Perspective and Challenges in Electrochemical Approaches for Reactive CO2 Separations. *iScience* **2021**, *24* (12), 103422. https://doi.org/10.1016/J.ISCI.2021.103422.

(52) Watkins, J. D.; Siefert, N. S.; Zhou, X.; Myers, C. R.; Kitchin, J. R.; Hopkinson, D. P.; Nulwala, H. B. Redox-Mediated Separation of Carbon Dioxide from Flue Gas. *Energy and Fuels* **2015**, *29* (11), 7508–7515. https://doi.org/10.1021/acs.energyfuels.5b01807.

(53) Xie, H.; Wu, Y.; Liu, T.; Wang, F.; Chen, B.; Liang, B. Low-Energy-Consumption Electrochemical CO2 Capture Driven by Biomimetic Phenazine Derivatives Redox Medium. *Appl Energy* **2020**, *259*, 114119. https://doi.org/10.1016/j.apenergy.2019.114119.

(54) Jin, S.; Wu, M.; Gordon, R. G.; Aziz, M. J.; Kwabi, D. G. PH Swing Cycle for CO2 Capture Electrochemically Driven through Proton-Coupled Electron Transfer. *Energy Environ Sci* **2020**, *13* (10), 3706–3722. https://doi.org/10.1039/d0ee01834a.

(55) Stern, M. C.; Simeon, F.; Herzog, H.; Alan Hatton, T. An Electrochemically-Mediated Gas Separation Process for Carbon Abatement. *Energy Procedia* **2013**, *37*, 1172–1179. https://doi.org/10.1016/j.egypro.2013.05.214.

(56) Wang, M.; Hariharan, S.; Shaw, R. A.; Hatton, T. A. Energetics of Electrochemically Mediated Amine Regeneration Process for Flue Gas CO2 Capture. *International Journal of Greenhouse Gas Control* **2019**, *82* (January), 48–58. https://doi.org/10.1016/j.ijggc.2018.12.028.

(57) Stern, M. C.; Simeon, F.; Herzog, H.; Hatton, T. A. Post-Combustion Carbon Dioxide Capture Using Electrochemically Mediated Amine Regeneration. *Energy Environ Sci* **2013**, *6* (8), 2505–2517. https://doi.org/10.1039/c3ee41165f.

(58) DuBois, D. L.; Miedaner, A.; Bell, W.; Smart, J. C. Electrochemical Concentration of Carbon Dioxide. In *Electrochemical and Electrocatalytic Reactions of Carbon Dioxide*; 1993; pp 94–117.

(59) Voskian, S.; Hatton, T. A. Faradaic Electro-Swing Reactive Adsorption for CO2 Capture. *Energy Environ Sci* **2019**, *12* (12), 3530–3547. https://doi.org/10.1039/c9ee02412c.

(60) Liu, Y.; Chow, C. M.; Phillips, K. R.; Wang, M.; Voskian, S.; Alan Hatton, T. Electrochemically Mediated Gating Membrane with Dynamically Controllable Gas Transport. *Sci Adv* **2020**, *6* (42), 22–24. https://doi.org/10.1126/sciadv.abc1741.

(61) Gurkan, B.; Simeon, F.; Hatton, T. A. Quinone Reduction in Ionic Liquids for Electrochemical CO2 Separation. *ACS Sustain Chem Eng* **2015**, *3* (7), 1394–1405. https://doi.org/10.1021/acssuschemeng.5b00116.

(62) Simpson, T. C.; Durand, R. R. Reactivity of Carbon Dioxide with Quinones. *Electrochim Acta* **1990**, *35* (9), 1399–1403. https://doi.org/10.1016/0013-4686(90)85012-C.

(63) Singh, P.; Rheinhardt, J. H.; Olson, J. Z.; Tarakeshwar, P.; Mujica, V.; Buttry, D. A. Electrochemical Capture and Release of Carbon Dioxide Using a Disulfide-Thiocarbonate Redox Cycle. *J Am Chem Soc* **2017**, *139* (3), 1033–1036. https://doi.org/10.1021/jacs.6b10806.

(64) Harris, D.; Bushnell, E. Density Functional Theory Study of the Capture and Release of Carbon Dioxide by Benzyl-Disulfide, -Diselenide, and -Ditelluride. *Journal of Physical Chemistry A* **2019**, *123* (15), 3383–3388. https://doi.org/10.1021/acs.jpca.9b01862.

(65) Ranjan, R.; Olson, J.; Singh, P.; Lorance, E. D.; Buttry, D. A.; Gould, I. R. Reversible Electrochemical Trapping of Carbon Dioxide Using 4,4′-Bipyridine That Does Not Require Thermal Activation. *Journal of Physical Chemistry Letters* **2015**, *6* (24), 4943–4946. https://doi.org/10.1021/acs.jpclett.5b02220.

(66) Ishida, H.; Ohba, T.; Yamaguchi, T.; Ohkubo, K. Interaction between CO2 and Electrochemically Reduced Species of N-Propyl-4,4′-Bipyridinium Cation. *Chemistry Letters*. 1994, pp 905–908. https://doi.org/10.1246/cl.1994.905.

(67) Zito, A. M.; Clarke, L. E.; Barlow, J. M.; Bím, D.; Zhang, Z.; Ripley, K. M.; Li, C. J.; Kummeth, A.; Leonard, M. E.; Alexandrova, A. N.; Brushett, F. R.; Yang, J. Y. Electrochemical Carbon Dioxide Capture and Concentration. *Chem Rev* **2023**, *123*, 8069–8098. https://doi.org/10.1021/acs.chemrev.2c00681.

(68) Barlow, J. M.; Clarke, L. E.; Zhang, Z.; Bím, D.; Ripley, K. M.; Zito, A.; Brushett, F. R.; Alexandrova, A. N.; Yang, J. Y. Molecular Design of Redox Carriers for Electrochemical CO 2 Capture and Concentration. *Chem Soc Rev* **2022**, *51*, 8415–8433. https://doi.org/10.1039/d2cs00367h.

(69) Li, X.; Zhao, X.; Liu, Y.; Hatton, T. A.; Liu, Y. Redox-Tunable Lewis Bases for Electrochemical Carbon Dioxide Capture. *Nat Energy* **2022**, *7*, 1065–1075. https://doi.org/10.1038/s41560-022-01137-z.

(70) Xie, H.; Jiang, W.; Liu, T.; Wu, Y.; Wang, Y.; Chen, B.; Niu, D.; Liang, B. Low-Energy Electrochemical Carbon Dioxide Capture Based on a Biological Redox Proton Carrier. *Cell Rep Phys Sci* **2020**, *1* (5), 100046. https://doi.org/10.1016/j.xcrp.2020.100046.

(71) Renfrew, S. E.; Starr, D. E.; Strasser, P. Electrochemical Approaches toward CO2 Capture and Concentration. *ACS Catal* **2020**, *10*, 13058–13074. https://doi.org/10.1021/acscatal.0c03639.

(72) Huang, C.; Liu, C.; Wu, K.; Yue, H.; Tang, S.; Lu, H.; Liang, B. CO2 Capture from Flue Gas Using an Electrochemically Reversible Hydroquinone/Quinone Solution. *Energy and Fuels* **2019**, *33* (4), 3380–3389. https://doi.org/10.1021/acs.energyfuels.8b04419.

(73) Jin, S.; Wu, M.; Jing, Y.; Gordon, R. G.; Aziz, M. J. Low Energy Carbon Capture via Electrochemically Induced PH Swing with Electrochemical Rebalancing. *Nat Commun* **2022**, *13*, 2140. https://doi.org/10.1038/s41467-022-29791-7.

(74) Pang, S.; Jin, S.; Yang, F.; Alberts, M.; Li, L.; Xi, D.; Gordon, R. G.; Wang, P.; Aziz, M. J.; Ji, Y. A Phenazine-Based High-Capacity and High-Stability Electrochemical CO2 Capture Cell with Coupled Electricity Storage. *Nat Energy* **2023**, *8* (10), 1126–1136. https://doi.org/10.1038/s41560-023-01347-z.

(75) Seo, H.; Rahimi, M.; Hatton, T. A. Electrochemical Carbon Dioxide Capture and Release with a Redox-Active Amine. *J Am Chem Soc* **2022**, *144* (5), 2164–2170. https://doi.org/10.1021/JACS.1C10656/ASSET/IMAGES/LARGE/JA1C10656_0006.JPEG.

(76) Rahimi, M.; Catalini, G.; Hariharan, S.; Wang, M.; Puccini, M.; Hatton, T. A. Carbon Dioxide Capture Using an Electrochemically Driven Proton Concentration Process. *Cell Rep Phys Sci* **2020**, *1* (4), 100033. https://doi.org/10.1016/J.XCRP.2020.100033.

(77) Yamaguchi, A.; Inuzuka, R.; Takashima, T.; Hayashi, T.; Hashimoto, K.; Nakamura, R. Regulating Proton-Coupled Electron Transfer for Efficient Water Splitting by Manganese Oxides at Neutral PH. *Nat Commun* **2014**, *5* (May), 1–6. https://doi.org/10.1038/ncomms5256.

(78) Quan, M.; Sanchez, D.; Wasylkiw, M. F.; Smith, D. K. Voltammetry of Quinones in Unbuffered Aqueous Solution: Reassessing the Roles of Proton Transfer and Hydrogen Bonding in the Aqueous Electrochemistry of Quinones. *J Am Chem Soc* **2007**, *129* (42), 12847–12856. https://doi.org/10.1021/ja0743083.

(79) Jing, Y.; Amini, K.; Xi, D.; Jin, S.; Alfaraidi, A.; Kerr, E. F.; Roy, G. Electrochemically Induced CO2 Capture Enabled by Aqueous Quinone Flow Chemistry. *ChemRxiv* **2023**, 1–13.

(80) Barlow, J. M.; Yang, J. Y. Oxygen-Stable Electrochemical CO2 Capture and Concentration with Quinones Using Alcohol Additives. *J Am Chem Soc* **2022**, *144* (31), 14161–14169. https://doi.org/10.1021/jacs.2c04044.

(81) Diederichsen, K. M.; Liu, Y.; Ozbek, N.; Seo, H.; Hatton, T. A. Toward Solvent-Free Continuous-Flow Electrochemically Mediated Carbon Capture with High-Concentration Liquid Quinone Chemistry. *Joule* **2022**, *6* (1), 221–239. https://doi.org/10.1016/j.joule.2021.12.001.

(82) Li, X.; Zhao, X.; Liu, Y.; Hatton, T. A.; Liu, Y. Redox-Tunable Lewis Bases for Electrochemical Carbon Dioxide Capture. *Nat Energy* **2022**, *7* (11), 1065–1075. https://doi.org/10.1038/s41560-022-01137-z.

(83) Anantharaman, R.; Bolland, O.; Booth, N.; Dorst, E. van; Vattenfall, C. E.; Fernandes, E. S.; Franco, F.; Milano, E. M. Polit. di; Milano, G. M. Polit. di; Nikolic, D.; Alstom, A. P.; Prins, M.; Rezvani, S.; Robinson, L. *D1. 4.3 European Best Practice Guidelines for Assessment of CO2 Capture Technologies.*; 2011.

(84) Nessi, E.; Papadopoulos, A. I.; Seferlis, P. A Review of Research Facilities, Pilot and Commercial Plants for Solvent-Based Post-Combustion CO2 Capture: Packed Bed, Phase-Change and Rotating Processes. *International Journal of Greenhouse Gas Control* **2021**, *111*, 103474.

(85) Chen, E.; Fulk, S.; Beaudry, M.; Lin, Y.-J.; Sachde, D.; Zhang, Y.; Stevens, K.; Nielsen, P.; Walters, M.; Liu, C.-T.; Wu, Y.; Akinpelumi, K.; Gao, T.; Selinger, J.; Suresh, A.; Rochelle, G. T.; Fisher, K.; Sexton, A.; Dombrowski, K.; Steen, W.; Farmer, K.; Bernau, M. *Evaluation of Concentrated Piperazine for CO2 Capture from Coal-Fired Flue Gas (Final Report, REV0)*; 2019. https://doi.org/doi:10.2172/1512446.

(86) Liu, A.; Musgrave, C. B.; Li, X.; Goddard, W. A.; Liu, Y. Non-Aqueous Alkoxide-Mediated Electrochemical Carbon Capture. *Nat Energy* **2024**. https://doi.org/10.1038/s41560-024-01614-7.

(87) Liu, Y.; Ye, H. Z.; Diederichsen, K. M.; Van Voorhis, T.; Hatton, T. A. Electrochemically Mediated Carbon Dioxide Separation with Quinone Chemistry in Salt-Concentrated Aqueous Media. *Nat Commun* **2020**, *11* (1), 1–11. https://doi.org/10.1038/s41467-020-16150-7.

(88) Aurbach, D. *Nonaqueous Electrochemistry*; Marcel Dekker, Inc., 1999.

(89) Nagaoka, T.; Nishii, N.; Fujii, K.; Ogura, K. Mechanisms of Reductive Addition of CO2 to Quinones in Acetonitrile. *Journal of Electroanalytical Chemistry* **1992**, *322*, 383–389. https://doi.org/10.1016/0022-0728(92)80090-Q.

(90) Mizen, M. B.; Wrighton, M. S. Reductive Addition of CO2 to 9,10-Phenanthrenequinone. *J Electrochem Soc* **1989**, *136* (4), 941–946.

(91) Namazian, M.; Zare, H. R.; Yousofian-Varzaneh, H. Electrochemical Behavior of Tetrafluoro-p-Benzoquinone at the Presence of Carbon Dioxide: Experimental and Theoretical Studies. *Electrochim Acta* **2016**, *196*, 692–698. https://doi.org/10.1016/j.electacta.2016.02.159.

(92) Qiao, X.; Li, D.; Cheng, L.; Jin, B. Mechanism of Electrochemical Capture of CO2 via Redox Cycle of Chlorinated 1,4-Naphthoquinone in BMIMBF4: An in-Situ FT-IR Spectroelectrochemical Approach. *Journal of Electroanalytical Chemistry* **2019**, *845* (May), 126–136. https://doi.org/10.1016/j.jelechem.2019.05.057.

(93) Yin, W.; Grimaud, A.; Azcarate, I.; Yang, C.; Tarascon, J. M. Electrochemical Reduction of CO2 Mediated by Quinone Derivatives: Implication for Li-CO2 Battery. *Journal of Physical Chemistry C* **2018**, *122* (12), 6546–6554. https://doi.org/10.1021/acs.jpcc.8b00109.

(94) Hikita, H.; Asai, S.; Ishikawa, H.; Honda, M. The Kinetics of Reactions of Carbon Dioxide with Monoethanolamine, Diethanolamine and Triethanolamine by a Rapid Mixing Method. *The Chemical Engineering Journal* **1977**, *13* (1), 7–12. https://doi.org/10.1016/0300-9467(77)80002-6.

(95) Versteeg, G. F.; Van Dijck, L. A. J.; Van Swaaij, W. P. M. On the Kinetics between CO2 and Alkanolamines Both in Aqueous and Non-Aqueous Solutions. An Overview. *Chem Eng Commun* **1996**, *144* (May), 133–158. https://doi.org/10.1080/00986449608936450.

(96) Afkhamipour, M.; Mofarahi, M. Sensitivity Analysis of the Rate-Based CO2 Absorber Model Using Amine Solutions (MEA, MDEA and AMP) in Packed Columns. *International Journal of Greenhouse Gas Control* **2014**, *25*, 9–22. https://doi.org/10.1016/j.ijggc.2014.03.005.

(97) Scovazzo, P.; Poshusta, J.; DuBois, D.; Koval, C.; Noble, R. Electrochemical Separation and Concentration of <1% Carbon Dioxide from Nitrogen. *J Electrochem Soc* **2003**, *150* (5), D91–D98. https://doi.org/10.1149/1.1566962.

(98) Seader, J. D.; Henley, E. J.; Roper, D. K. *Separation Process Principles with Applications Using Process Simulators*, Fourth Edi.; John Wiley & Sons, Inc, 2016.

(99) Boualavong, J.; Papakonstantinou, K. G.; Gorski, C. A. Determining Desired Sorbent Properties for Proton-Coupled Electron Transfer-Controlled CO2 Capture Using an Adaptive Sampling-Refined Classifier. *Chem Eng Sci* **2023**, *274*, 118673. https://doi.org/10.1016/j.ces.2023.118673.

(100) Pinsent, B. R. W.; Pearson, L.; Roughton, F. J. W. THE KINETICS OF COMBINATION OF CARBON DIOXIDE WITH HYDROXIDE IONS. *Transactions of the Faraday Society* **1956**, *52*, 1512–1520.

(101) Wallin, M.; Olausson, S. Simultaneous Absorption of H2S and CO2 into a Solution of Sodium Carbonate. *Chem Eng Commun* **1993**, *123*, 43–59. https://doi.org/10.1080/00986449308936164.

(102) Mitchell, M. J.; Jensen, O. E.; Cliffe, K. A.; Maroto-Valer, M. M. A Model of Carbon Dioxide Dissolution and Mineral Carbonation Kinetics. *Proceedings of the Royal Society A: Mathematical, Physical and Engineering Sciences* **2010**, *466* (2117), 1265–1290. https://doi.org/10.1098/rspa.2009.0349.

(103) Boualavong, J.; Gorski, C. A. Kinetic Drawbacks of Combining Electrochemical CO2 Sorbent Reactivation with CO2 Absorption. *Ind Eng Chem Res* **2023**, *62* (46), 19784–19800. https://doi.org/10.1021/acs.iecr.3c02204.

(104) Wolf-Gladrow, D. A.; Zeebe, R. E.; Klaas, C.; Körtzinger, A.; Dickson, A. G. Total Alkalinity: The Explicit Conservative Expression and Its Application to Biogeochemical Processes. *Mar Chem* **2007**, *106* (1-2 SPEC. ISS.), 287–300. https://doi.org/10.1016/j.marchem.2007.01.006.

(105) Bottoms, R. R. Process for Separating Acidic Gases. 1783901, 1930.

(106) Rochelle, G. T. Amine Scrubbing for CO2 Capture. *Science (1979)* **2009**, *325*, 1652–1654.

(107) Conway, W.; Wang, X.; Fernandes, D.; Burns, R.; Lawrance, G.; Puxty, G.; Maeder, M. Comprehensive Kinetic and Thermodynamic Study of the Reactions of CO2(Aq) and HCO3- with Monoethanolamine (MEA) in Aqueous Solution. *Journal of Physical Chemistry A* **2011**, *115* (50), 14340–14349. https://doi.org/10.1021/jp2081462.

(108) Hikita, H.; Ishikawa, H.; Uku, K.; Murakami, T. Diffusivities of Mono-, Di-, and Triethanolamines in Aqueous Solutions. *J Chem Eng Data* **1980**, *25* (4), 324–325. https://doi.org/10.1021/je60087a008.

(109) Arachchige, U. S. P. R.; Aryal, N.; Eimer, D. A.; Melaaen, M. C. Viscosities of Pure and Aqueous Solutions of Monoethanolamine (MEA), Diethanolamine (DEA) and N-Methyldiethanolamine (MDEA). *Annual Transactions of the Nordic Rheology Society* **2013**, *21*, 299–306.

(110) Jayarathna, S. A.; Weerasooriya, A.; Dayarathna, S.; Eimer, D. A.; Melaaen, M. C. Densities and Surface Tensions of CO2 Loaded Aqueous Monoethanolamine Solutions with r = (0.2 to 0.7) at T = (303.15 to 333.15) K. *Journal of Chemical Engineering Data* **2013**, *58*, 986–992.

(111) Mores, P.; Scenna, N.; Mussati, S. A Rate Based Model of a Packed Column for CO2 Absorption Using Aqueous Monoethanolamine Solution. *International Journal of Greenhouse Gas Control* **2012**, *6*, 21–36. https://doi.org/10.1016/j.ijggc.2011.10.012.

(112) Dugas, R. E. Pilot-Plant Study of Carbon Dioxide Capture by Aqueous Monoethanolamine, The University of Texas at Austin, 2006.

(113) Pintola, T.; Tontiwachwuthikul, P.; Meisen, A. Simulation of Pilot Plant and Industrial CO2-MEA Absorbers. *Gas Separation and Purification* **1993**, *7* (1), 47–52. https://doi.org/10.1016/0950-4214(93)85019-R.

(114) DeMontigny, D.; Aboudheir, A.; Tontiwachwuthikul, P.; Chakma, A. Modelling the Performance of a CO2 Absorber Containing Structured Packing. *Ind Eng Chem Res* **2006**, *45* (8), 2594–2600. https://doi.org/10.1021/ie050567u.

(115) Tontiwachwuthikul, P.; Meisen, A.; Lim, C. J. Novel Pilot Plant Technique for Sizing Gas Absorbers with Chemical Reactions. *Can J Chem Eng* **1989**, *67* (4), 602–607. https://doi.org/10.1002/cjce.5450670412.

(116) Øi, L. E.; Brathen, T.; Berg, C.; Brekne, S. K.; Flatin, M.; Johnsen, R.; Moen, I. G.; Thomassen, E. Optimization of Configurations for Amine Based CO2 Absorption Using Aspen HYSYS. *Energy Procedia* **2014**, *51* (1876), 224–233. https://doi.org/10.1016/j.egypro.2014.07.026.

(117) De Leye, L.; Froment, G. F. Rigorous Simulation and Design of Columns for Gas Absorption and Chemical Reaction. *Comput Chem Eng* **1986**, *10* (5), 493–504. https://doi.org/10.1016/0098-1354(86)85017-7.

(118) Lawal, A.; Wang, M.; Stephenson, P.; Yeung, H. Dynamic Modelling of CO2 Absorption for Post Combustion Capture in Coal-Fired Power Plants. *Fuel* **2009**, *88* (12), 2455–2462. https://doi.org/10.1016/j.fuel.2008.11.009.

(119) Henley, E. J.; Seader, J. D. *Equilibrium-Stage Separation Operations in Chemical Engineering*; Wiley: New York, 1981.

(120) Kenig, E. Y.; Schneider, R.; Górak, A. Reactive Absorption: Optimal Process Design via Optimal Modelling. *Chem Eng Sci* **2001**, *56* (2), 343–350. https://doi.org/10.1016/S0009-2509(00)00234-7.

(121) Putta, K. R.; Tobiesen, F. A.; Svendsen, H. F.; Knuutila, H. K. Applicability of Enhancement Factor Models for CO2 Absorption into Aqueous MEA Solutions. *Appl Energy* **2017**, *206*, 765–783. https://doi.org/10.1016/j.apenergy.2017.08.173.

(122) Wellek, R. M.; Brunson, R. J.; Law, F. H. Enhancement Factors for Gas-absorption with Second-order Irreversible Chemical Reaction. *Can J Chem Eng* **1978**, *56* (2), 181–186. https://doi.org/10.1002/cjce.5450560205.

(123) Towler, G.; Sinnott, R. *Chemical Engineering Design: Principles, Practice, and Economics of Plant and Process Design*, 1st ed.; 2008.

(124) Kvamsdal, H. M.; Rochelle, G. T. Effects of the Temperature Bulge in CO2 Absorption from Flue Gas by Aqueous Monoethanolamine. *Ind Eng Chem Res* **2008**, *47* (3), 867–875. https://doi.org/10.1021/ie061651s.

(125) Mangalapally, H. P.; Hasse, H. Pilot Plant Experiments for Post Combustion Carbon Dioxide Capture by Reactive Absorption with Novel Solvents. *Energy Procedia* **2011**, *4*, 1–8. https://doi.org/10.1016/j.egypro.2011.01.015.

(126) Strigle Jr., R. F. *Random Packings and Packed Towers: Design and Applications*; Gulf Publishing Company: Houston, TX, 1987.

(127) Kister, H. Z.; Gill, D. R. Flooding and Pressure Drop Prediction for Structured Packings. *Institution of Chemical Engineers Symposium Series* **1992**, *128*, A109-123.

(128) Noeres, C.; Kenig, E. Y.; Górak, A. Modelling of Reactive Separation Processes: Reactive Absorption and Reactive Distillation. *Chemical Engineering and Processing* **2003**, *42* (3), 157–178. https://doi.org/10.1016/S0255-2701(02)00086-7.

(129) Saimpert, M.; Puxty, G.; Qureshi, S.; Wardhaugh, L.; Cousins, A. A New Rate Based Absorber and Desorber Modelling Tool. *Chem Eng Sci* **2013**, *96*, 10–25. https://doi.org/10.1016/j.ces.2013.03.013.

(130) Liang, Z. H.; Sanpasertparnich, T.; Tontiwachwuthikul, P. P.; Gelowitz, D.; Idem, R. Part 1: Design, Modeling and Simulation of Post-Combustion CO2 Capture Systems Using Reactive Solvents. *Carbon Manag* **2011**, *2* (3), 265–288. https://doi.org/10.4155/cmt.11.19.

(131) Pandya, J. D. Adiabatic Gas Absorption and Stripping with Chemical Reaction in Packed Towers. *Chem Eng Commun* **1983**, *19* (4–6), 343–361. https://doi.org/10.1080/00986448308956351.

(132) Treybal, R. E. Adiabatic Gas Absorption and Stripping in Packed Towers. *Ind Eng Chem* **1969**, *61* (7), 36–41.

(133) Tobiesen, F. A.; Svendsen, H. F.; Juliussen, O. Experimental Validation of a Rigorous Absorber Model for CO2 Postcombustion Capture. *AIChE Journal* **2007**, *53* (4), 846–865. https://doi.org/10.1002/aic.

(134) Mathur, V. K.; Wellek, R. M. Effect of Axial Dispersion on Interphase Mass Transfer in Packed Absorption Columns. *Can J Chem Eng* **1976**, *54* (1–2), 90–96. https://doi.org/10.1002/cjce.5450540113.

(135) Brittan, M. I.; Woodburn, E. T. The Influence of Axial Dispersion on Carbon Dioxide Absorption Tower Performance. *AIChE Journal* **1966**, *12* (3), 541–548. https://doi.org/10.1002/aic.690120327.

(136) Norouzbahari, S.; Shahhosseini, S.; Ghaemi, A. Chemical Absorption of CO2 into an Aqueous Piperazine (PZ) Solution: Development and Validation of a Rigorous Dynamic Rate-Based Model. *RSC Adv* **2016**, *6* (46), 40017–40032. https://doi.org/10.1039/c5ra27869d.

(137) Linek, V.; Sinkule, J.; Havelka, P. Empirical Design Method Of Industrial Carbon Dioxide-Mixed Solvent Absorbers with Axial Dispersion in Gas. *Ind Eng Chem Res* **1994**, *33* (11), 2731–2737. https://doi.org/10.1021/ie00035a024.

(138) Bachmann, P.; Bück, A.; Tsotsas, E. Investigation of the Residence Time Behavior of Particulate Products and Correlation for the Bodenstein Number in Horizontal Fluidized Beds. *Powder Technol* **2016**, *301*, 1067–1076. https://doi.org/10.1016/j.powtec.2016.07.045.

(139) Onda, K.; Takeuchi, H.; Okumoto, Y. Mass Transfer Coefficients Between Gas and Liquid Phases in Packed Columns. *Journal of Chemical Engineering of Japan* **1968**, *1* (1), 56–62.

(140) Hanley, B.; Chen, C.-C. New Mass-Transfer Correlations for Packed Towers. *AIChE Journal* **2011**, *58* (1), 132–152. https://doi.org/10.1002/aic.

(141) Billet, R.; Schultes, M. Prediction of Mass Transfer Columns with Dumped and Arranged Packings: Updated Summary of the Calculation Method of Billet and Schultes. *Chemical Engineering Research and Design* **1999**, *77* (6), 498–504. https://doi.org/10.1205/026387699526520.

(142) Greer, T.; Bedelbayev, A.; Igreja, J. M.; Gomes, J. F.; Lie, B. A Simulation Study on the Abatement of CO2 Emissions by De-Absorption with Monoethanolamine. *Environ Technol* **2010**, *31* (1), 107–115. https://doi.org/10.1080/09593330903373764.

(143) Tontiwachwuthikul, P.; Meisen, A.; Lim, C. J. CO2 Absorption by NaOH, Monoethanolamine and 2-Amino-2-Methyl-1-Propanol Solutions in a Packed Column. *Chem Eng Sci* **1992**, *47* (2), 381–390. https://doi.org/10.1016/0009-2509(92)80028-B.

(144) Khan, F. M.; Krishnamoorthi, V.; Mahmud, T. Modelling Reactive Absorption of CO2 in Packed Columns for Post-Combustion Carbon Capture Applications. *Chemical Engineering Research and Design* **2011**, *89* (9), 1600–1608. https://doi.org/10.1016/j.cherd.2010.09.020.

(145) Faramarzi, L.; Kontogeorgis, G. M.; Michelsen, M. L.; Thomsen, K.; Stenby, E. H. Absorber Model for CO2 Capture by Monoethanolamine. *Ind Eng Chem Res* **2010**, *49* (8), 3751–3759. https://doi.org/10.1021/ie901671f.

(146) Jayarathna, S. A.; Lie, B.; Melaaen, M. C. Amine Based CO2 Capture Plant: Dynamic Modeling and Simulations. *International Journal of Greenhouse Gas Control* **2013**, *14*, 282–290. https://doi.org/10.1016/j.ijggc.2013.01.028.

(147) Mores, P.; Scenna, N.; Mussati, S. Post-Combustion CO2 Capture Process: Equilibrium Stage Mathematical Model of the Chemical Absorption of CO2 into Monoethanolamine (MEA) Aqueous Solution. *Chemical Engineering Research and Design* **2011**, *89* (9), 1587–1599. https://doi.org/10.1016/j.cherd.2010.10.012.

(148) Mores, P.; Scenna, N.; Mussati, S. CO2 Capture Using Monoethanolamine (MEA) Aqueous Solution: Modeling and Optimization of the Solvent Regeneration and CO2 Desorption Process. *Energy* **2012**, *45* (1), 1042–1058. https://doi.org/10.1016/J.ENERGY.2012.06.038.

(149) Madeddu, C.; Errico, M.; Baratti, R. *Process Modeling in Aspen Plus®*; 2019. https://doi.org/10.1007/978-3-030-04579-1_2.

(150) Biliyok, C.; Lawal, A.; Wang, M.; Seibert, F. Dynamic Modelling, Validation and Analysis of Post-Combustion Chemical Absorption CO2 Capture Plant. *International Journal of Greenhouse Gas Control* **2012**, *9* (2012), 428–445. https://doi.org/10.1016/j.ijggc.2012.05.001.

(151) Wang, C. Mass Transfer Coefficients and Effective Area of Packing. Ph.D. Thesis, The University of Texas at Austin, 2015.

(152) Xu, Y.; Zheng, M.; Musgrave, C. B.; Zhang, L.; Goddard, W. A.; Bukowski, B. C.; Liu, Y. Assessing the Kinetics of Quinone-CO2 Adduct Formation for Electrochemically Mediated Carbon Capture. *ACS Sustain Chem Eng* **2023**, *11*, 11333–11341. https://doi.org/10.1021/acssuschemeng.3c03321.

(153) Darling, R. M.; Gallagher, K. G.; Kowalski, J. A.; Ha, S.; Brushett, F. R. Pathways to Low-Cost Electrochemical Energy Storage: A Comparison of Aqueous and Nonaqueous Flow Batteries. *Energy Environ Sci* **2014**, *7* (11), 3459–3477. https://doi.org/10.1039/c4ee02158d.

(154) Pahlevaninezhad, M.; Leung, P.; Velasco, P. Q.; Pahlevani, M.; Walsh, F. C.; Roberts, E. P. L.; Ponce de León, C. A Nonaqueous Organic Redox Flow Battery Using Multi-Electron Quinone Molecules. *J Power Sources* **2021**, *500*, 229942. https://doi.org/10.1016/j.jpowsour.2021.229942.

(155) Geysens, P.; Li, Y.; Vankelecom, I.; Fransaer, J.; Binnemans, K. Highly Soluble 1,4-Diaminoanthraquinone Derivative for Nonaqueous Symmetric Redox Flow Batteries. *ACS Sustain Chem Eng* **2020**, *8* (9), 3832–3843. https://doi.org/10.1021/acssuschemeng.9b07244.

(156) Pahari, S. K.; Gokoglan, T. C.; Chaurasia, S.; Bolibok, J. N.; Golen, J. A.; Agar, E.; Cappillino, P. J. Toward High-Performance Nonaqueous Redox Flow Batteries through Electrolyte Design. *ACS Appl Energy Mater* **2023**, *6* (14), 7521–7534. https://doi.org/10.1021/acsaem.3c00910.

(157) Yang, B.; Hoober-Burkhardt, L.; Krishnamoorthy, S.; Murali, A.; Prakash, G. K. S.; Narayanan, S. R. High-Performance Aqueous Organic Flow Battery with Quinone-Based Redox Couples at Both Electrodes. *J Electrochem Soc* **2016**, *163* (7), A1442–A1449. https://doi.org/10.1149/2.1371607jes.

(158) Zhang, S.; Li, X.; Chu, D. An Organic Electroactive Material for Flow Batteries. *Electrochim Acta* **2016**, *190*, 737–743. https://doi.org/10.1016/j.electacta.2015.12.139.

(159) Wikner, E.; Thiringer, T. Extending Battery Lifetime by Avoiding High SOC. *Applied Sciences (Switzerland)* **2018**, *8*, 1825. https://doi.org/10.3390/app8101825.

(160) Roe, S.; Menictas, C.; Skyllas-Kazacos, M. A High Energy Density Vanadium Redox Flow Battery with 3 M Vanadium Electrolyte. *J Electrochem Soc* **2016**, *163* (1), A5023–A5028. https://doi.org/10.1149/2.0041601jes.

(161) Kiani, A.; Jiang, K.; Feron, P. Techno-Economic Assessment for CO2 Capture From Air Using a Conventional Liquid-Based Absorption Process. *Front Energy Res* **2020**, *8*, 1–13. https://doi.org/10.3389/fenrg.2020.00092.

(162) Choi, J.; Cho, H.; Yun, S.; Jang, M. G.; Oh, S. Y.; Binns, M.; Kim, J. K. Process Design and Optimization of MEA-Based CO2 Capture Processes for Non-Power Industries. *Energy* **2019**, *185*, 971–980. https://doi.org/10.1016/j.energy.2019.07.092.

(163) Zito, A. M.; Bím, D.; Vargas, S.; Alexandrova, A. N.; Yang, J. Y. Computational and Experimental Design of Quinones for Electrochemical CO2 Capture and Concentration. *ACS Sustain Chem Eng* **2022**, *10* (34), 11387–11395. https://doi.org/10.1021/acssuschemeng.2c03463.

(164) Barker, G. Chapter 11 - Towers. In *The Engineer's Guide to Plant Layout and Piping Design for the Oil and Gas Industries*; Gulf Professional Publishing, 2018; pp 285–308.

(165) *World's Largest Crude Column Installed (Video)*. Process Consulting Services Inc. https://www.revamps.com/news/worlds-largest-crude-column-installed (accessed 2024-08-21).

(166) Huynh, M. T.; Anson, C. W.; Cavell, A. C.; Stahl, S. S.; Hammes-Schiffer, S. Quinone 1 e– and 2 e–/2 H+ Reduction Potentials: Identification and Analysis of Deviations from Systematic Scaling Relationships. *J Am Chem Soc* **2016**, *138*, 15903–15910. https://doi.org/10.1021/JACS.6B05797.

(167) Zhang, Z.; Kummeth, A. L.; Yang, J. Y.; Alexandrova, A. N. Inverse Molecular Design of Alkoxides and Phenoxides for Aqueous Direct Air Capture of CO2. *Proc Natl Acad Sci U S A* **2022**, *119* (25), 1–11. https://doi.org/10.1073/pnas.2123496119.

12. For Table of Contents Only